J. Fluid Mech. (2011), *vol.* 669, *pp.* 298–327. © Cambridge University Press 2011
doi:10.1017/S0022112010005045

Dynamics of uncharged colloidal inclusions in polyelectrolyte hydrogels

ALIASGHAR MOHAMMADI AND REGHAN J. HILL†

Department of Chemical Engineering, McGill University, Montreal, Quebec H3A 2B2, Canada

(Received 3 February 2010; revised 12 September 2010; accepted 23 September 2010; first published online 14 January 2011)

We calculate the dynamics of an uncharged colloidal sphere embedded in a quenched polyelectrolyte hydrogel to (i) an oscillatory (optical and magnetic) force, as adopted in classical micro-rheology, and (ii) an oscillatory electric field, as adopted in electrical micro-rheology and electro-acoustics. The hydrogel is modelled as a linearly elastic porous medium with the charge fixed to the skeleton and saturated with a Newtonian electrolyte; and the colloidal inclusion is modelled as a rigid, impenetrable sphere. The dynamic micro-rheological susceptibility, defined as the ratio of the particle displacement to the strength of an applied oscillatory force, depends on the fixed-charge density and ionic strength and is bounded by the limits for incompressible and uncharged, compressible skeletons. Nevertheless, the influences of fixed charge and ionic strength vanish at frequencies above the reciprocal draining time, where the polymer and the electrolyte hydrodynamically couple as a single incompressible phase. Generally, the effects of fixed charge and ionic strength are small compared with, for example, the influences of polymer slip at the particle surface. The electrical susceptibility, defined as the ratio of the particle displacement to the strength of an applied oscillatory electric field, is directly influenced by charge at all frequencies, irrespective of skeleton compressibility. At low frequencies, polymer charge modulates the driving (electro-osmotic) and restoring (electrostatically enhanced elastic) forces, whereas charge has no influence on the restoring force at high frequencies where dilational strain is suppressed by hydrodynamic coupling with the electrolyte. In striking contrast to charged inclusions in uncharged hydrogels (Wang & Hill, *J. Fluid Mech.*, vol. 640, 2009, pp. 357–400), the electrical susceptibility at high frequencies is independent of electrolyte concentration. Rather, the dynamics primarily reflect the elastic modulus, charge and hydrodynamic permeability, with a relatively weak dependence on particle size. Interestingly, the dynamic mobility in the zero-momentum reference frame, which is central to the electro-acoustic response, is qualitatively different from the dynamic mobility in the skeleton-fixed reference frame. Finally, we propose a phenomenological harmonic-oscillator model to address – in an approximate manner – the dynamics of charged particles in charged hydrogels. This shows that particle dynamics at low frequencies are dominated by particle charge, whereas high-frequency dynamics are dominated by hydrogel charge.

Key words: colloids, convection in porous media, micro-/nano-fluid dynamics

† Email address for correspondence: reghan.hill@mcgill.ca

https://doi.org/10.1017/S0022112010005045 Published online by Cambridge University Press

1. Introduction

There have been long-standing efforts in the literature to probe the microstructure and bulk properties of complex fluids, including hydrogels. More recently, viscoelastic properties of complex fluids have been obtained via the response of colloidal inclusions to external forces. These micro-rheological tools exploit optical, magnetic or gravitational forces (active methods) and thermal forces (passive methods) to perturb the inclusions and use linear response theory to furnish mechanical properties from experimentally measured susceptibilities (see the reviews by MacKintosh & Schmidt 1999; Gardel, Valentine & Weitz 2005; Waigh 2005).

The generalized Stokes–Einstein relation (GSER), which provides a relationship between the susceptibility of a sphere in a viscoelastic medium and its Brownian fluctuations was first derived by Zwanzig & Bixon (1970) and later applied to micro-rheology by Mason & Weitz (1995). Accounting for skeleton compressibility and, thus, hydrodynamic draining, Levine & Lubensky (2000, 2001) showed that the GSER is a good approximation in the intermediate range of frequencies where the (incompressible) fluid and elastic-network dynamics couple, but inertia can still be neglected.

Outstanding questions concerning the validity of the GSER pertain to electrostatic interactions, which are long-ranged and almost always present (see the review by Squires & Mason 2010). Using mode-coupling theory, for example, Nägele (2003) identified a breakdown of the GSER for a charged colloidal sphere in a dispersion of charge-stabilized colloidal particles. More recently, Mohammadi & Hill (2010) studied the influences of fixed-charge density of polyelectrolyte hydrogels on the steady susceptibility of uncharged colloidal inclusions. They showed that the steady susceptibility transits between compressible limits for the uncharged polymer skeleton and an incompressible limit in which electrostatic interactions are strong enough to completely arrest polymer dilation. In both cases, the shear modulus is set by the intrinsic elasticity of the uncharged polymer skeleton. However, these calculations were limited to steady deformation, whereas most micro-rheological experiments probe dynamics at frequencies in the range of 0.1 to 100 kHz. In this paper, we extend the analysis of Mohammadi & Hill (2010) to more realistic dynamical situations.

As highlighted by an extensive literature on the electrokinetics of colloidal particles in Newtonian fluids (Russel, Schowalter & Saville 1989) and the more recent studies of colloidal dynamics in viscoelastic porous media (Hill & Ostoja-Starzewski 2008), electric fields drive electro-osmotic flow. The coupling of electrical and hydrodynamic forces, which are influenced by ion electro-migration and diffusion, make the interpretation of electro-micro-rheological data much more challenging than that of their classical counterparts. Accordingly, only a few experimental studies have been reported (Mizuno, Kimura & Hayakawa 2001, 2004).

Most micro-rheological techniques are well suited for very soft, fragile viscoelastic media. The extension to stiffer materials requires technological advances, e.g. larger excitation forces (Kollmannsberger & Fabry 2007) and less noisy instrumentation (Nugent-Glandorf & Perkins 2004; Klein *et al.* 2007). With the exception of diffusing-wave spectroscopy (Mason & Weitz 1995), micro-rheological methods are generally limited to transparent materials.

To address these limitations, Wang & Hill (2009) recently proposed electro-acoustics as a diagnostic tool for dispersions of colloidal inclusions in hydrogels. They undertook extensive theoretical calculations for charged inclusions in uncharged polymer skeletons, showing that electro-acoustic experiments, which probe the

https://doi.org/10.1017/S0022112010005045 Published online by Cambridge University Press

dynamic electrophoretic mobility of the inclusions, could yield a measurable response in the ultrasound frequency range for materials that have elastic moduli of several hundred megapascals. Their proposed experimental methodology involves the same instrumentation as the electro-acoustic instruments used for characterizing colloidal suspensions and emulsions (O'Brien 1988, 1990; Hunter 1998; Dukhin *et al.* 2000; Dukhin & Goetz 2001).

Most biological hydrogels and, indeed, many synthetic hydrogels bear fixed charge. It therefore remains to examine how this charge affects the electro-acoustic response. Although we have not included charge on the colloidal inclusions in this study, when combined with the calculations of Wang & Hill (2009), the results may help to discern the relative contributions of particle and polymer charge to the micro-rheological susceptibility.

Lai, Hou & Mow (1991) and Gu, Lai & Mow (1998) used tri- and multi-phasic theories (assuming electro-neutrality) to derive dynamical equations for charged soft tissues. Their models were advanced in later studies (Li, Chen & Lam 2004*a*, 2006; Li *et al.* 2004*b*) by adopting the Poisson equation to handle electrostatics. Similar modelling was undertaken by Tanaka and co-workers in the context of gel phase transitions (English, Tanaka & Edelman 1997). They followed earlier studies of Tanaka, Hocker & Benedek (1973) and Tanaka, Ishiwata & Ishimoto (1977) to analyse light-scattering experiments that furnish hydrogel viscoelastic properties from diffusive polymer dynamics in an otherwise-quiescent fluid.

Johnson (1982) addressed interacting fluid and polymer motions separately by generalizing the well-known Biot theory for acoustics in porous media to hydrogels. In contrast to Tanaka *et al.* (1973), he showed that shear modes propagate and that attenuation is important. Pride (1994) derived equations governing electromagnetic and acoustic coupling in porous media. He also provided transport coefficients – and derived Onsager reciprocity relationships – for averaged equations governing the propagation of elastic and electrical waves. Even though his work concerned fluid-saturated sedimentary rocks with fixed charge on the solid surfaces, Pride's theory is closely connected to the electro-acoustics of polyelectrolyte hydrogels. Similar connections exist between Levine and Lubensky's (2000, 2001) micro-rheological theory for uncharged gels and Biot's model for fluid-saturated geological formations.

In this paper, we derive analytical solutions to the model of Mohammadi & Hill (2010) for charged compressible hydrogels, but with terms that capture the dynamical micro-scale draining under oscillatory forcing. To furnish tractable analytical solutions for compressible hydrogels, we neglect fluid inertia and temporal changes in electrolyte concentration. Nevertheless, we include these terms in a separate analysis for incompressible gels, targeting the high-frequency response where the fluid and polymer couple as a single incompressible phase. This incompressible model furnishes an accurate solution of the full model at frequencies above the reciprocal draining time and is therefore particularly valuable for interpreting the high-frequency (ultrasound) electro-acoustic response.

The paper is organized as follows. We begin in § 2 by presenting the linearized multi-phase electrokinetic model in frequency space. Section 3 provides details of the solution methodology. We examine the results in § 4, showing how various parameters influence the micro-rheological, electrical and electro-acoustic responses. This section also presents a phenomenological harmonic-oscillator model to briefly address the influence of particle charge and furnish simple closed-form approximations for the dynamics at asymptotically low and high frequencies. Finally, § 5 provides a concluding summary.

https://doi.org/10.1017/S0022112010005045 Published online by Cambridge University Press

2. Electrokinetic model

We extend the model of Mohammadi & Hill (2010) to account for harmonic dynamics. A single rigid impenetrable uncharged colloidal sphere is embedded in a polyelectrolyte hydrogel. The hydrogel is modelled by coupling the Poisson equation with conservation equations for N mobile ions, fluid momentum, polymer momentum, fluid mass and polymer mass. In the usual manner, we write the dependent variables as the sum of an equilibrium value and a small perturbation. Thus, under oscillatory forcing with angular frequency ω, each variable has the general form, e.g. $\psi = \psi^\circ + \psi'(\boldsymbol{r})\mathrm{e}^{-\mathrm{i}\omega t}$, where t and $\boldsymbol{r}$ are the time and the position, respectively; the superscript $\circ$ denotes equilibrium values, and the primes denote perturbations. Note that all equilibrium quantities are constants in this work, because the inclusion is uncharged, and the polymer is assumed statistically homogeneous. With an incompressible electrolyte and small polymer volume fraction, the full model, linearized for small perturbations from equilibrium, comprises

$$-\epsilon_o\epsilon_s\nabla^2\psi' = \rho^{m\prime} + \rho^{f\prime}, \tag{2.1}$$

$$-\mathrm{i}\omega n_j' = -\nabla\cdot\left(-D_j\nabla n_j' - z_j\mathrm{e}\frac{D_j}{k_BT}n_j^\circ\nabla\psi' + n_j^\circ\boldsymbol{u}'\right) \quad (j = 1, \ldots, N), \tag{2.2}$$

$$-\rho\mathrm{i}\omega\boldsymbol{u}' = \eta\nabla^2\boldsymbol{u}' - \nabla p' - \frac{\eta}{\ell^2}(\boldsymbol{u}' + \mathrm{i}\omega\boldsymbol{v}') - \rho^{m\circ}\nabla\psi', \tag{2.3}$$

$$0 = \frac{\mathscr{E}}{2(1+\nu)}\left[\nabla^2\boldsymbol{v}' + \frac{1}{1-2\nu}\nabla(\nabla\cdot\boldsymbol{v}')\right] + \frac{\eta}{\ell^2}(\boldsymbol{u}' + \mathrm{i}\omega\boldsymbol{v}') - \rho^{f\circ}\nabla\psi', \tag{2.4}$$

$$\nabla\cdot\boldsymbol{u}' = 0, \tag{2.5}$$

$$\rho^{f\prime} = -\rho^{f\circ}\nabla\cdot\boldsymbol{v}', \tag{2.6}$$

where the mobile-charge density perturbation $\rho^{m\prime} = \sum_{j=1}^{N} n_j' z_j \mathrm{e}$.

In the Poisson equation (2.1), $\epsilon_o\epsilon_s$ is the solvent dielectric constant; ψ is the electrostatic potential; and ρ^m and ρ^f are, respectively, the mobile- and fixed-charge densities. Note that mobile ions include counterions of the fixed charge and ions from the added salt. In the N ion conservation equations (2.2), D_j, z_j and n_j are, respectively, the jth ion diffusion coefficient, valance and concentration, and $\boldsymbol{u}$ is the fluid velocity; k_BT and e are, respectively, the thermal energy and the fundamental charge. In the fluid momentum conservation equation (2.3), ρ and η are the fluid density and shear viscosity; p is the pressure; ℓ is the Brinkman screening length (square root of the Darcy permeability); and $\boldsymbol{v}$ is the polymer-skeleton displacement. Finally, in the polymer momentum conservation equation (2.4), $\mathscr{E}$ and ν are, respectively, the polymer-skeleton Young's modulus and the Poisson ratio.

Equations (2.5) and (2.6) are, respectively, fluid (electrolyte solvent) and polymer mass conservation equations; the latter couples polymer-skeleton dilation $\nabla\cdot\boldsymbol{v}'$ with the uniform equilibrium fixed-charge density $\rho^{f\circ}$. Boundary conditions ensure an impenetrable particle surface without fluid or polymer slip, and the particle equation of motion is satisfied by linearly superposing the disturbances from two independent sub-problems, both of which are detailed below.

3. Dynamic electrical and micro-rheological susceptibilities

We calculate perturbations to equilibrium in a stationary particle reference frame. Using standard procedures, two linearly independent sub-problems are solved, and

https://doi.org/10.1017/S0022112010005045 Published online by Cambridge University Press

their solutions are superposed to satisfy the particle equation of motion, with an appropriate correction for transferring the particle and fluid to an accelerating reference frame.

In the Z-problem, the far-field polymer and electrolyte are displaced a distance $-\boldsymbol{Z}$ in the absence of an applied electric field ($\boldsymbol{E}=0$). The boundary conditions are $\boldsymbol{v}'=0$ and $\boldsymbol{u}'=0$ at $r=a$ and $\boldsymbol{v}'\to-\boldsymbol{Z}$, $\boldsymbol{u}'\to \mathrm{i}\omega\boldsymbol{Z}$ and $\nabla p'\to-\rho\omega^2\boldsymbol{Z}$ as $r\to\infty$. In the E-problem, the particle is fixed at the origin ($\boldsymbol{Z}=0$) in the presence of an external, harmonically oscillating electric field $\boldsymbol{E}$. The boundary conditions are $\boldsymbol{v}'=0$ and $\boldsymbol{u}'=0$ at $r=a$ and $\boldsymbol{v}'\to 0$, $\boldsymbol{u}'\to-(\ell^2/\eta)\rho^{f\circ}\boldsymbol{E}$ and $\nabla p'\to-\mathrm{i}\omega\rho(\ell^2/\eta)\rho^{f\circ}\boldsymbol{E}$ as $r\to\infty$. The boundary conditions for the electrostatic potential are $\epsilon_\circ\epsilon_p(\nabla_<\psi')\cdot\boldsymbol{e}_r-\epsilon_\circ\epsilon_s(\nabla_>\psi')\cdot\boldsymbol{e}_r=0$ and ψ' continuous at $r=a$; $\psi'\to-\boldsymbol{E}\cdot\boldsymbol{r}$ (E-problem) and 0 (Z-problem) as $r\to\infty$; and ψ' finite at $r=0$. The subscripts of the gradient operator distinguish the particle ($<$) and solvent sides ($>$) of the interface. Other boundary conditions (see Mohammadi & Hill 2010) include $\boldsymbol{j}_j\cdot\hat{\boldsymbol{n}}=0$ at $r=a$ and $\rho^{m\prime}\to 0$ and $\rho^{f\prime}\to 0$ as $r\to\infty$.

The total force on the stationary particle is the sum of the forces $\boldsymbol{F}^Z$ and $\boldsymbol{F}^E$ from the foregoing Z-problem and E-problem. However, for a freely translating particle under the influence of an electric field, the equation of motion becomes

$$-\rho_p V_p\omega^2\boldsymbol{Z}=-\rho V_p\omega^2\boldsymbol{Z}+\boldsymbol{F}^Z+\boldsymbol{F}^E, \tag{3.1}$$

where ρ_p is the particle density and $V_p=(4/3)\pi a^3$ is the particle volume. As detailed in Appendix A, (3.1) includes particle inertia and a correction for changing the reference frame upon superposing the Z-problem and the E-problem.

By linearity and symmetry, the forces on the stationary particle can be written (O'Brien & White 1978):

$$\boldsymbol{F}^E=f^E\boldsymbol{E}\quad\text{and}\quad\boldsymbol{F}^Z=f^Z\boldsymbol{Z}, \tag{3.2}$$

where f^E and f^Z, which are independent of E and Z, are furnished by analytical solutions of (2.1)–(2.6) and their boundary conditions. In general, $\boldsymbol{F}^E$ has contributions from electrical, hydrodynamic and elastic stresses. However, the direct electrical force is zero here because the particle bears no charge; the hydrodynamic and elastic (mechanical-contact) forces are, respectively,

$$\boldsymbol{F}^h=\int_{r=a}\boldsymbol{\sigma}^h\cdot\boldsymbol{e}_r\,\mathrm{d}A\quad\text{and}\quad\boldsymbol{F}^m=\int_{r=a}\boldsymbol{\sigma}^e\cdot\boldsymbol{e}_r\,\mathrm{d}A, \tag{3.3}$$

where $\boldsymbol{\sigma}^h$ and $\boldsymbol{\sigma}^e$ are the Newtonian hydrodynamic and linearly elastic stress tensors. In the usual manner, the divergence theorem applied to the integrals above gives

$$\boldsymbol{F}^h+\boldsymbol{F}^m=-\int_V\nabla\cdot(\boldsymbol{\sigma}^h+\boldsymbol{\sigma}^e)\,\mathrm{d}V+\int_{r\to\infty}(\boldsymbol{\sigma}^h+\boldsymbol{\sigma}^e)\cdot\boldsymbol{e}_r\,\mathrm{d}A, \tag{3.4}$$

where V is the volume enclosed by the particle surface at $r=a$ and a large concentric sphere with radius $r\to\infty$. In the absence of polymer inertia, $\nabla\cdot(\boldsymbol{\sigma}^h+\boldsymbol{\sigma}^e)=-\mathrm{i}\omega\rho\boldsymbol{u}$, where the electrical body force $-(\rho^m+\rho^f)\nabla\psi=0$ when we are concerned with the linear response (O'Brien & White 1978; Yariv 2006).

From (3.1), the dynamic electrical susceptibility is

$$\frac{Z}{E}=\frac{f^E}{(\rho-\rho_p)\omega^2V_p-f^Z}, \tag{3.5}$$

where the terms involving V_p can be neglected at low frequencies, i.e. in the absence of particle and fluid inertia. Note that the dynamic mobility $U/E=-\mathrm{i}\omega Z/E$, where

https://doi.org/10.1017/S0022112010005045 Published online by Cambridge University Press

U is the particle velocity, is not the same dynamic electrophoretic mobility defined by O'Brien (1988) to interpret electro-acoustic dynamics. As detailed in Appendix A, μ_E demands a vanishing far-field pressure gradient and, hence, vanishing far-field fluid velocity; it yields a steady particle displacement at zero frequency that corresponds to a steady translation of the skeleton in a stationary undisturbed fluid. We will therefore examine the particle dynamics, as given by (3.5), in the stationary skeleton reference frame with finite far-field pressure gradient and fluid acceleration.

As detailed in Appendix B, the equation of motion when the particle is subjected to an external force $\boldsymbol{F}$ in the absence of an electric field is

$$-\rho_p V_p \omega^2 \boldsymbol{Z} = -\rho V_p \omega^2 \boldsymbol{Z} + \boldsymbol{F}^Z + \boldsymbol{F}, \tag{3.6}$$

so the dynamic susceptibility is

$$\frac{Z}{F} = \frac{1}{(\rho - \rho_p)\omega^2 V_p - f^Z}. \tag{3.7}$$

3.1. *Low-frequency dynamics*

Here we provide an analytical solution of (2.1)–(2.6) and their boundary conditions. Recall that the model is simplified for low frequencies where temporal dynamics are solely due to hydrodynamic coupling of the electrolyte fluid and elastic polymer skeleton. This solution includes polymer dilation, which, in turn, produces electrical-charge density perturbations that influence electro-osmotic flow and dynamically stiffen the polymer. Inertial and temporal ion-concentration perturbations are addressed in § 3.2, where we examine high-frequency dynamics under conditions where the polymer is necessarily incompressible because of strong hydrodynamic coupling with the (incompressible) electrolyte.

The velocity and displacement fields in the particle-fixed reference frame can be written:

$$\boldsymbol{u}'^X = \nabla \times \boldsymbol{\Psi}^X + \boldsymbol{u}^X_\infty, \tag{3.8}$$

$$\boldsymbol{v}'^X = \nabla \times \boldsymbol{\Phi}^X + \nabla \phi^X + \boldsymbol{v}^X_\infty, \tag{3.9}$$

where $\nabla \cdot \boldsymbol{\Psi}^X = 0$, $\nabla \cdot \boldsymbol{\Phi}^X = 0$ and $\nabla \phi^X \to 0$ as $r \to \infty$. Also, $\boldsymbol{u}^Z_\infty = \mathrm{i}\omega \boldsymbol{Z}$, $\boldsymbol{u}^E_\infty = -\rho^{f\circ}(\ell^2/\eta)\boldsymbol{E}$, $\boldsymbol{v}^Z_\infty = -\boldsymbol{Z}$ and $\boldsymbol{v}^E_\infty = 0$. Note that the superscripts $X \in \{Z, E\}$ identify the Z-problem and the E-problem.

Substituting $\rho^{f\prime}$ from (2.6) into (2.1), taking the divergence and curl of (2.3) and (2.4) and using (2.5), (3.8) and (3.9) give

$$\epsilon_o \epsilon_s \nabla^2 \psi'^X = -\rho^{m\prime X} + \rho^{f\circ} \nabla^2 \phi^X, \tag{3.10}$$

$$-\nabla^2 p'^X = \mathrm{i}\omega \frac{\eta}{\ell^2} \nabla^2 \phi^X + \rho^{m\circ} \nabla^2 \psi'^X, \tag{3.11}$$

$$\eta \nabla^2 \nabla \times \nabla \times \boldsymbol{\Psi}^X = \frac{\eta}{\ell^2} \nabla \times \nabla \times \boldsymbol{\Psi}^X + \mathrm{i}\omega \frac{\eta}{\ell^2} \nabla \times \nabla \times \boldsymbol{\Phi}^X, \tag{3.12}$$

$$0 = \frac{\mathscr{E}(1-\nu)}{(1+\nu)(1-2\nu)} \nabla^2 \nabla^2 \phi^X - \rho^{f\circ} \nabla^2 \psi'^X + \mathrm{i}\omega \frac{\eta}{\ell^2} \nabla^2 \phi^X, \tag{3.13}$$

$$0 = \frac{\mathscr{E}}{2(1+\nu)} \nabla^2 \nabla \times \nabla \times \boldsymbol{\Phi}^X + \mathrm{i}\omega \frac{\eta}{\ell^2} \nabla \times \nabla \times \boldsymbol{\Phi}^X + \frac{\eta}{\ell^2} \nabla \times \nabla \times \boldsymbol{\Psi}^X, \tag{3.14}$$

$$\nabla^2 n_j'^X + \frac{z_j \mathrm{e}}{k_B T} n_j^\circ \nabla^2 \psi'^X = 0. \tag{3.15}$$

https://doi.org/10.1017/S0022112010005045 Published online by Cambridge University Press

Following Mohammadi & Hill (2010), (3.15) simplifies to

$$\nabla^2 \rho^{m\prime X} = -\frac{2Ie^2}{k_B T} \nabla^2 \psi^{\prime X}, \tag{3.16}$$

where $I = (1/2)\sum_j n_j^\circ z_j^2$ is the ionic strength, which includes counterions of the fixed polymer charge and ions of the added salt.

Decoupling (3.10), (3.13) and (3.16) yields the biharmonic equation for the mobile-charge density perturbation:

$$(\nabla^2 + K^2)(\nabla^2 + L^2)\rho^{m\prime X} = 0, \tag{3.17}$$

where the wavenumbers K and L satisfy

$$K^2 + L^2 = -D^2 + \mathrm{i}\delta^2 \quad \text{and} \quad (KL)^2 = -\mathrm{i}(\delta\kappa)^2 \tag{3.18}$$

with

$$\delta^2 = \frac{\omega\eta(1-2\nu)(1+\nu)}{\mathscr{E}\ell^2(1-\nu)} \quad \text{and} \quad D^2 = \kappa^2 + \frac{\beta^2(1-2\nu)(1+\nu)}{1-\nu} \tag{3.19}$$

and

$$\kappa^2 = \frac{2I\mathrm{e}^2}{k_B T \epsilon_o \epsilon_s} \quad \text{and} \quad \beta^2 = \frac{\rho^{f\circ 2}}{\epsilon_o \epsilon_s \mathscr{E}}. \tag{3.20}$$

Note that κ^{-1} is the well-known Debye screening length and β^{-1} is the distance over which electrostatic repulsion among fixed charges due to polymer dilation is balanced by the accompanying elastic stresses (Mohammadi & Hill 2010). Moreover, D^{-1} is an effective Debye length, modified for the fixed-charge density perturbations that accompany skeleton dilation (Mohammadi & Hill 2010), and δ^{-1} is a length scale associated with skeleton compressibility. Introduced by Tanaka *et al.* (1973) and de Gennes (1976), δ^{-1} identifies the crossover (draining) frequency ($\delta a = 1$) at which the fluid and an uncharged porous solid couple as a single incompressible phase (Levine & Lubensky 2001). With a stationary undisturbed fluid, Tanaka *et al.* (1973) and de Gennes (1976) showed that polymer density fluctuations diffuse with the diffusion coefficient

$$D_g = \omega\delta^{-2} = \frac{\mathscr{E}\ell^2(1-\nu)}{\eta(1-2\nu)(1+\nu)}. \tag{3.21}$$

In our model, the wavenumber δ and its accompanying crossover frequency are modulated by electrostatic repulsion among fixed charges on the polymer skeleton. These influences are quantified by the wavenumbers K and L that, we will see, correspond to outward-propagating, damped compressional waves.

By linearity and symmetry, $\rho^{m\prime X} = \hat{\rho}^{mX}(r)\boldsymbol{X}\cdot\boldsymbol{e}_r$, so (3.17) simplifies to

$$(\mathscr{L} + K^2)(\mathscr{L} + L^2)\hat{\rho}^{mX}(r) = 0, \tag{3.22}$$

where

$$\mathscr{L}\cdot = \frac{\mathrm{d}}{\mathrm{d}r}\left[\frac{1}{r^2}\frac{\mathrm{d}}{\mathrm{d}r}(r^2\cdot)\right]. \tag{3.23}$$

Since $K^2 \neq L^2$, and $\rho^{m\prime X} \to 0$ as $r \to \infty$, the density perturbations are

$$\rho^{m\prime X} = \left[C_1^X h_1^{(1)}(K_1 r) + C_2^X h_1^{(1)}(L_1 r)\right]\boldsymbol{X}\cdot\boldsymbol{e}_r, \tag{3.24}$$

where $h_1^{(1)}(K_1 r) = -(\mathrm{i} + K_1 r)\mathrm{e}^{\mathrm{i}K_1 r}/(K_1 r)^2$ is the spherical Hankel function of first kind and K_1 and L_1 are, respectively, the square roots of K^2 and L^2 with $\mathrm{Im}(K_1) > 0$

https://doi.org/10.1017/S0022112010005045 Published online by Cambridge University Press

and $\mathrm{Im}(L_1) > 0$. Note that the constants C_1^X and C_2^X are specified by the boundary conditions.

Next, by linearity and symmetry, $\psi'^X = \hat{\psi}^X(r)\boldsymbol{X}\cdot\boldsymbol{e}_r$, so (3.16) and (3.24) give

$$\psi'^X = -\left(\frac{k_BT}{2I\mathrm{e}^2}\right)\rho^{m\prime X} + \left(\frac{1}{3}C_3^X r + \frac{C_4^X}{r^2}\right)\boldsymbol{X}\cdot\boldsymbol{e}_r, \tag{3.25}$$

where the constants C_3^X and C_4^X are specified by the boundary conditions. Since $\psi'^Z \to 0$ and $\psi'^E \to -\boldsymbol{E}\cdot\boldsymbol{r}$ as $r\to\infty$, $C_3^Z = 0$ and $C_3^E = -3$.

The electrostatic potential inside the particle $\psi_{in}^X(\boldsymbol{r},t) = \psi_{in}^\circ + \psi_{in}'^X(\boldsymbol{r})\mathrm{e}^{-\mathrm{i}\omega t}$ satisfies Laplace's equation

$$\nabla^2\psi'^X = 0 \tag{3.26}$$

when $r < a$. Since ψ'^X is linear in $\boldsymbol{X}$ and finite at $r = 0$,

$$\psi'^X = B_0^X - B_1^X\boldsymbol{X}\cdot\boldsymbol{r} \tag{3.27}$$

when $r < a$. Continuity of ψ'^X at the particle surface ($r = a$) requires

$$B_0^X = 0 \text{ and } B_1^X = -\frac{k_BT}{2I\mathrm{e}^2}\left[C_1^X h_1^{(1)}(K_1a)/a + C_2^X h_1^{(1)}(L_1a)/a\right] - C_3^X/3 - C_4^X/a^3, \tag{3.28}$$

and continuity of the normal component of the electric field at $r = a$ requires

$$(\epsilon_p/\epsilon_s)B_1^X = \frac{k_BT}{2I\mathrm{e}^2}\left[C_1^X\frac{\mathrm{d}}{\mathrm{d}r}\left(h_1^{(1)}(K_1r)\right)_{r=a} + C_2^X\frac{\mathrm{d}}{\mathrm{d}r}\left(h_1^{(1)}(L_1r)\right)_{r=a}\right] - C_3^X/3 + 2C_4^X/a^3. \tag{3.29}$$

Note that a vanishing normal ion flux at $r = a$ demands $C_4^Z = 0$ and $C_4^E = -a^3/2$.

The irrotational part of the displacement $\phi^X = \hat{\phi}^X(r)\boldsymbol{X}\cdot\boldsymbol{e}_r$ is furnished by (3.10), (3.24) and (3.25), giving

$$\phi^X = \left[-\frac{C_1^X}{\rho^{f\circ}}h_1^{(1)}(K_1r)\left(\frac{1}{\kappa^2}+\frac{1}{K^2}\right) - \frac{C_2^X}{\rho^{f\circ}}h_1^{(1)}(L_1r)\left(\frac{1}{\kappa^2}+\frac{1}{L^2}\right) + \frac{1}{3}C_5^X r + \frac{C_6^X}{r^2}\right]\boldsymbol{X}\cdot\boldsymbol{e}_r, \tag{3.30}$$

where $C_5^X = 0$ ensures that $\nabla\phi^X \to 0$ as $r\to\infty$.

Having now determined ψ'^X, $\rho^{m\prime X}$ and ϕ^X from (3.10), (3.13) and (3.15) and their boundary conditions, let us now consider the pressure. Again, by linearity and symmetry, $p'^X = \hat{p}^X(r)\boldsymbol{X}\cdot\boldsymbol{e}_r$, so (3.11), (3.24), (3.25) and (3.30) give

$$\begin{aligned} p'^X = {} & \left(C_1^X\left[\mathrm{i}\omega\frac{\eta}{\ell^2}\frac{1}{\rho^{f\circ}}\left(\frac{1}{\kappa^2}+\frac{1}{K^2}\right) + \rho^{m\circ}\frac{k_BT}{2I\mathrm{e}^2}\right]h_1^{(1)}(K_1r)\right. \\ & \left. + C_2^X\left[\mathrm{i}\omega\frac{\eta}{\ell^2}\frac{1}{\rho^{f\circ}}\left(\frac{1}{\kappa^2}+\frac{1}{L^2}\right) + \rho^{m\circ}\frac{k_BT}{2I\mathrm{e}^2}\right]h_1^{(1)}(L_1r) + \frac{C_7^X}{3}r + \frac{C_p^X}{r^2}\right)\boldsymbol{X}\cdot\boldsymbol{e}_r, \end{aligned} \tag{3.31}$$

where $C_7^X = 0$ ensures that $p' \to 0$ as $r\to\infty$.

Next, the characteristic equation furnishing the solenoidal part of the displacement $\nabla\times\boldsymbol{\Phi}^X$ from (3.12) and (3.14) is

$$(\nabla^2 + m^2)\nabla^2(\nabla\times\nabla\times\boldsymbol{\Phi}^X) = 0, \tag{3.32}$$

where

$$m^2 = \ell^{-2}[2\mathrm{i}\omega\eta(1+\nu)/\mathscr{E} - 1]. \tag{3.33}$$

The wavenumber m has values m_1 and m_2 with $\mathrm{Im}(m_1) > 0$. The associated transverse wave, introduced by Tanaka *et al.* (1973), identifies m_1^{-1} as the penetration depth

https://doi.org/10.1017/S0022112010005045 Published online by Cambridge University Press

beyond which fluid motion relative to the polymer skeleton is suppressed by friction. Note that the wavenumber K associated with the compressional modes is modulated by electrostatic interactions, whereas the transverse wave with the wavenumber m is the same as for uncharged skeletons (Levine & Lubensky 2001; Fu, Shenoy & Powers 2008).

Using the identity $\boldsymbol{\Phi}^X = \nabla \times [f^X(r)\boldsymbol{X}]$, (3.32) simplifies to

$$(\mathscr{L} + m^2)\mathscr{L}\mathscr{L} f_r^X(r) = 0, \tag{3.34}$$

so with $\nabla \times \boldsymbol{\Phi}^X \to 0$ as $r \to \infty$, the decaying solution is

$$f_r^X = \frac{C_8^X}{m^4} h_1^{(1)}(m_1 r) - \frac{1}{2} C_v^X + \frac{C_9^X}{r^2}, \tag{3.35}$$

giving

$$\nabla \times \boldsymbol{\Phi}^X = -2\left[\frac{C_8^X}{m^4}\frac{h_1^{(1)}(m_1 r)}{r} - \frac{1}{2}\frac{C_v^X}{r} + \frac{C_9^X}{r^3}\right]\boldsymbol{X}\cdot\boldsymbol{e}_r\boldsymbol{e}_r - \left[\frac{C_8^X}{m^4}\frac{1}{r}\frac{\mathrm{d}}{\mathrm{d}r}\left(r h_1^{(1)}(m_1 r)\right) - \frac{1}{2}\frac{C_v^X}{r} - \frac{C_9^X}{r^3}\right]\boldsymbol{X}\cdot\boldsymbol{e}_\theta\boldsymbol{e}_\theta. \tag{3.36}$$

From (3.9) and (3.36), the displacement $\boldsymbol{v}'$ satisfying the no-slip boundary condition $\boldsymbol{v}' = 0$ at $r = a$ yields

$$\frac{C_1^X}{\rho^{f\circ}}\left[\frac{\mathrm{d}}{\mathrm{d}r}\left(h_1^{(1)}(K_1 r)\right)\right]_{r=a}\left(\frac{1}{\kappa^2} + \frac{1}{K^2}\right) + \frac{C_2^X}{\rho^{f\circ}}\left[\frac{\mathrm{d}}{\mathrm{d}r}\left(h_1^{(1)}(L_1 r)\right)\right]_{r=a}\left(\frac{1}{\kappa^2} + \frac{1}{L^2}\right) + 2\frac{C_8^X}{m^4}\frac{h_1^{(1)}(m_1 a)}{a} - \frac{C_v^X}{a} + 2\frac{\alpha^X}{a^3} = \lambda_v^X, \tag{3.37}$$

$$\frac{C_1^X}{\rho^{f\circ}}\frac{h_1^{(1)}(K_1 a)}{a}\left(\frac{1}{\kappa^2} + \frac{1}{K^2}\right) + \frac{C_2^X}{\rho^{f\circ}}\frac{h_1^{(1)}(L_1 a)}{a}\left(\frac{1}{\kappa^2} + \frac{1}{L^2}\right) + \frac{C_8^X}{m^4}\frac{1}{a}\left[\frac{\mathrm{d}}{\mathrm{d}r}\left(r h_1^{(1)}(m_1 r)\right)\right]_{r=a} - \frac{1}{2}\frac{C_v^X}{a} - \frac{\alpha^X}{a^3} = \lambda_v^X, \tag{3.38}$$

where $\lambda_v^Z = -1$, $\lambda_v^E = 0$ and $\alpha^X = C_6^X + C_9^X$.

The characteristic equation for the fluid velocity, obtained by decoupling (3.12) and (3.14), is

$$(\nabla^2 + m^2)\nabla^2(\nabla \times \nabla \times \boldsymbol{\Psi}^X) = 0. \tag{3.39}$$

Applying a similar methodology to obtain $\boldsymbol{\Phi}^X$ gives

$$\nabla \times \boldsymbol{\Psi}^X = -2\left[\frac{C_{10}^X}{m^4}\frac{h_1^{(1)}(m_1 r)}{r} - \frac{1}{2}\frac{C_u^X}{r} + \frac{C_{11}^X}{r^3}\right]\boldsymbol{X}\cdot\boldsymbol{e}_r\boldsymbol{e}_r - \left[\frac{C_{10}^X}{m^4}\frac{1}{r}\frac{\mathrm{d}}{\mathrm{d}r}\left(r h_1^{(1)}(m_1 r)\right) - \frac{1}{2}\frac{C_u^X}{r} - \frac{C_{11}^X}{r^3}\right]\boldsymbol{X}\cdot\boldsymbol{e}_\theta\boldsymbol{e}_\theta, \tag{3.40}$$

https://doi.org/10.1017/S0022112010005045 Published online by Cambridge University Press

so from (3.8) and (3.40), the velocity $\boldsymbol{u}'$ satisfying the no-slip boundary condition $\boldsymbol{u}'=0$ at $r=a$ yields

$$-2\frac{C_{10}^X}{m^4}\frac{h_1^{(1)}(m_1a)}{a}+\frac{C_u^X}{a}-2\frac{C_{11}^X}{a^3}=\lambda_u^X, \tag{3.41}$$

$$-\frac{C_{10}^X}{m^4}\frac{1}{a}\left[\frac{\mathrm{d}}{\mathrm{d}r}\left(rh_1^{(1)}(m_1r)\right)\right]_{r=a}+\frac{1}{2}\frac{C_u^X}{a}+\frac{C_{11}^X}{a^3}=\lambda_u^X, \tag{3.42}$$

where $\lambda_u^Z=-\mathrm{i}\omega$ and $\lambda_u^E=\rho^{f\circ}\eta/\ell^2$.

Having now established the general functional form of all the fields based on symmetry and linearity, we must specify the remaining unknown constants from the governing equations and boundary conditions.

The fluid and polymer momentum conservation equations give

$$C_p^X-\eta C_u^X+\frac{\eta}{\ell^2}C_{11}^X+\mathrm{i}\omega\frac{\eta}{\ell^2}\alpha^X=\rho^{f\circ}C_4^X, \tag{3.43}$$

$$\mathrm{i}\omega C_v^X+C_u^X=0, \tag{3.44}$$

$$\frac{\mathscr{E}}{2(1+\nu)}C_8^X+\eta C_{10}^X=0, \tag{3.45}$$

$$\frac{\mathscr{E}}{2(1+\nu)}C_v^X+\frac{\eta}{\ell^2}C_{11}^X+\mathrm{i}\omega\frac{\eta}{\ell^2}\alpha^X=\rho^{f\circ}C_4^X. \tag{3.46}$$

Finally, from the far-field decays of $\boldsymbol{u}'$, $\boldsymbol{v}'$ and p' as $r\to\infty$,

$$\boldsymbol{F}^X=-\frac{4}{3}\pi\left(C_p^X+\frac{\mathscr{E}}{(1+\nu)}C_v^X+2\eta C_u^X\right)\boldsymbol{X}=-4\pi C_p^X\boldsymbol{X}, \tag{3.47}$$

so the micro-rheological and electrical susceptibilities are

$$\frac{Z}{F}=\frac{1}{4\pi C_p^Z}\quad\text{and}\quad\frac{Z}{E}=\frac{C_p^E}{C_p^Z}, \tag{3.48}$$

where

$$C_p^Z=-\frac{3}{2}\mu a\left[\frac{(1-2\nu)}{(1-\nu)}\frac{\beta_1(L_1)(K^2+\kappa^2)+\beta_1(K_1)(L^2+\kappa^2)}{\gamma_1(K^2+\kappa^2)-\gamma_2(L^2+\kappa^2)}\kappa^2+m^2\ell^2\right] \tag{3.49}$$

and

$$C_p^E=-\frac{1}{2}\mathrm{i}\mu a\frac{\epsilon_\circ\epsilon_s}{\rho^{f\circ}}\left[(K^2+\kappa^2)\left(B_1^E\beta_1(L_1)-\frac{3}{2}\beta_3(L_1)\right)\right.$$
$$\left.-(L^2+\kappa^2)\left(B_1^E\beta_1(K_1)-\frac{3}{2}\beta_3(K_1)\right)+6\mathrm{i}(1+\nu)\beta^2\ell^2\right], \tag{3.50}$$

with

$$B_1^E=\frac{3}{2}\frac{1}{(K^2+\kappa^2)\gamma_1+(L^2+\kappa^2)\gamma_2}\left[-4\beta^2\kappa^2\frac{a}{m_1}\frac{(1+\nu)(1-2\nu)}{(1-\nu)}\right.$$
$$\left.+\gamma_3(K^2+\kappa^2)-\gamma_4(L^2+\kappa^2)\right], \tag{3.51}$$

https://doi.org/10.1017/S0022112010005045 Published online by Cambridge University Press

$$\gamma_1 = \beta_1(L_1)\beta_2(L_1, K_1), \tag{3.52}$$

$$\gamma_2 = \beta_1(K_1)\beta_2(K_1, L_1), \tag{3.53}$$

$$\gamma_3 = \beta_2(L_1, K_1)\beta_3(L_1), \tag{3.54}$$

$$\gamma_4 = \beta_2(K_1, L_1)\beta_3(K_1) \tag{3.55}$$

and

$$\beta_1(x) = \frac{x^2a^2 + \mathrm{i}(2 + \epsilon_p/\epsilon_s)xa - (2 + \epsilon_p/\epsilon_s)}{-L^2(K_1a + \mathrm{i}) + K^2(L_1a + \mathrm{i})}, \tag{3.56}$$

$$\beta_2(x, y) = x^2(y^2a^2 + 4\mathrm{i}ya - 4) - \mathrm{i}\delta^2\kappa^2(m^2a^2 + 2\mathrm{i}m_1a - 2)/m^2 - \frac{\kappa^2(1 - 2\nu)}{m^2\ell^2(1 - \nu)}, \tag{3.57}$$

$$\beta_3(x) = \frac{x^2a^2 + 2\mathrm{i}xa - 2}{-L^2(K_1a + \mathrm{i}) + K^2(L_1a + \mathrm{i})}. \tag{3.58}$$

3.2. *High-frequency dynamics*

Here we present analytical solutions of the Z-problem and the E-problem with inertial and temporal ion-concentration perturbations. Because the dynamics in the frequency range in which these contributions cannot be neglected occur in the absence of polymer dilation, we simplify the problem by dealing with an intrinsically incompressible polymer skeleton from the outset. Accordingly, to remove singularities in the polymer equation of motion, we adopt the expansion (Hill & Ostoja-Starzewski 2008)

$$\boldsymbol{v}' = \boldsymbol{v}_0 + \epsilon\boldsymbol{v}_1 + \epsilon^2\boldsymbol{v}_2 + \ldots, \tag{3.59}$$

where $\nabla \cdot \boldsymbol{v}_0 \to 0$ as $\epsilon = 1 - 2\nu \to 0$. Moreover, using the well-known Helmholtz theorem from § 3.1, $\boldsymbol{u}'$ and $\boldsymbol{v}'$ have the same functional form.

Boundary conditions are the same as in § 3.1, but fluid inertia requires far-field pressure to satisfy

$$\nabla p'^{Z} \to -\omega^2\rho\boldsymbol{Z} \quad \text{and} \quad \nabla p'^{E} \to -\mathrm{i}\omega\rho\rho^{f\circ}(\ell^2/\eta)\boldsymbol{E} \quad \text{as} \quad r \to \infty. \tag{3.60}$$

Similar to § 3.1, the governing equations are

$$\epsilon_o\epsilon_s\nabla^2\psi'^{X} = -\rho^{m'X}, \tag{3.61}$$

$$\left(\nabla^2 + \mathrm{i}\frac{\omega}{D_s}\right)\rho^{m'X} = -\frac{2I\mathrm{e}^2}{k_BT}\nabla^2\psi'^{X}, \tag{3.62}$$

$$-\nabla^2 p'^{X} = \rho^{m\circ}\nabla^2\psi'^{X}, \tag{3.63}$$

$$\eta\nabla^2\nabla \times \nabla \times \boldsymbol{\Psi}^X = \frac{\eta}{\ell^2}(\nabla \times \nabla \times \boldsymbol{\Psi}^X + \mathrm{i}\omega\nabla \times \nabla \times \boldsymbol{\Phi}^X) - \mathrm{i}\omega\rho\nabla \times \nabla \times \boldsymbol{\Psi}^X, \tag{3.64}$$

$$\mu\nabla^2\nabla \cdot \boldsymbol{v}_1^X = \rho^{f\circ}\nabla^2\psi'^{X}, \tag{3.65}$$

$$\mu\nabla^2\nabla \times \nabla \times \boldsymbol{\Phi}^X = -\frac{\eta}{\ell^2}(\mathrm{i}\omega\nabla \times \nabla \times \boldsymbol{\Phi}^X + \nabla \times \nabla \times \boldsymbol{\Psi}'^{X}), \tag{3.66}$$

where $\mu = \mathscr{E}/[2(1 + \nu)]$ is the shear modulus. Note that $\rho^{f\prime} = 0$ because the polymer dynamics are incompressible, and to obtain a tractable analytical solution, we have set equal mobile-ion diffusivities, $D_j = D_s$.

https://doi.org/10.1017/S0022112010005045 Published online by Cambridge University Press

Equation (3.62) gives

$$\rho^{m\prime X} = C_1^{\prime X} h_1^{(1)}(M_1 r)\boldsymbol{X}\cdot\boldsymbol{e}_r \quad \text{and} \quad \psi^{\prime X} = \frac{1}{\epsilon_o\epsilon_s M^2}\rho^{m\prime X} + \left(\frac{C_2^{\prime X}}{3}r + \frac{C_3^{\prime X}}{r^2}\right)\boldsymbol{X}\cdot\boldsymbol{e}_r, \quad (3.67)$$

where M_1 is the square root of $M^2 = \mathrm{i}\omega/D_s - \kappa^2$ with $\mathrm{Im}(M_1) > 0$. The constants are specified by the electrostatic and ion-flux boundary conditions applied in § 3.1, which show that the charge density and electrostatic potential perturbations vanish in the Z-problem, i.e. $\rho^{m\prime Z} = \psi^{\prime Z} = 0$. Accordingly, electrolyte characteristics do not influence the susceptibility. In the E-problem, however, $\rho^{m\prime E}$ and $\psi^{\prime E}$ are finite, so the dynamic mobility does indeed depend on electrolyte characteristics.

From (3.63), (3.65) and (3.67),

$$p^{\prime X} = \frac{\rho^{f\circ}}{\epsilon_o\epsilon_s M^2}\rho^{m\prime X} + \left(\frac{C_4^{\prime X}}{3}r + \frac{C_p^{\prime X}}{r^2}\right)\boldsymbol{X}\cdot\boldsymbol{e}_r, \quad (3.68)$$

$$\nabla\cdot\boldsymbol{v}_1^X = \frac{\rho^{f\circ}}{\epsilon_o\epsilon_s\mu M^2}\rho^{m\prime X} + \frac{C_{v1}^{\prime X}}{r^2}\boldsymbol{X}\cdot\boldsymbol{e}_r. \quad (3.69)$$

Note that there is no need to calculate $\boldsymbol{v}_1^X$, because the force depends only on $\nabla\cdot\boldsymbol{v}_1$, which is closely linked to the pressure (Hill & Ostoja-Starzewski 2008). Moreover, $p^{\prime X}$ and $\nabla\cdot\boldsymbol{v}_1^X$ have an osmotic contribution that depends on the ionic strength and fixed-charge density.

Decoupling (3.64) and (3.66) gives

$$\begin{aligned}\boldsymbol{u}^{\prime X} = {} & 2\left[\frac{C_5^{\prime X}}{q^2 r}h_1^{(1)}(q_1 r) + \frac{C_6^{\prime X}}{s^2 r}h_1^{(1)}(s_1 r) - \frac{C_u^{\prime X}}{r^3}\right]\boldsymbol{X}\cdot\boldsymbol{e}_r\boldsymbol{e}_r \\ & + \left[\frac{C_5^{\prime X}}{q^2 r}\frac{\mathrm{d}}{\mathrm{d}r}\left(r h_1^{(1)}(q_1 r)\right) + \frac{C_6^{\prime X}}{s^2 r}\frac{\mathrm{d}}{\mathrm{d}r}\left(r h_1^{(1)}(s_1 r)\right) + \frac{C_u^{\prime X}}{r^3}\right]\boldsymbol{X}\cdot\boldsymbol{e}_\theta\boldsymbol{e}_\theta + \boldsymbol{u}_\infty^X, \quad (3.70)\end{aligned}$$

$$\begin{aligned}\boldsymbol{v}_0^X = {} & 2\left[\frac{C_7^{\prime X}}{q^2 r}h_1^{(1)}(q_1 r) + \frac{C_8^{\prime X}}{s^2 r}h_1^{(1)}(s_1 r) - \frac{C_{v0}^{\prime X}}{r^3}\right]\boldsymbol{X}\cdot\boldsymbol{e}_r\boldsymbol{e}_r \\ & + \left[\frac{C_7^{\prime X}}{q^2 r}\frac{\mathrm{d}}{\mathrm{d}r}\left(r h_1^{(1)}(q_1 r)\right) + \frac{C_8^{\prime X}}{s^2 r}\frac{\mathrm{d}}{\mathrm{d}r}\left(r h_1^{(1)}(s_1 r)\right) + \frac{C_{v0}^{\prime X}}{r^3}\right]\boldsymbol{X}\cdot\boldsymbol{e}_\theta\boldsymbol{e}_\theta + \boldsymbol{v}_\infty^X, \quad (3.71)\end{aligned}$$

where q^2 and s^2, and their respective square roots q_1 and s_1 with $\mathrm{Im}(q_1) > 0$ and $\mathrm{Im}(s_1) > 0$, satisfy

$$q^2 + s^2 = \mathrm{i}(\omega/\mu)(\eta/\ell^2) - 1/\ell^2 + \mathrm{i}\omega\rho/\eta \quad \text{and} \quad (qs)^2 = -(\omega^2/\mu)(\rho/\ell^2). \quad (3.72)$$

Note that q_1 and s_1 are the wavenumbers for two transverse waves. The wave s is associated with fluid-polymer viscous friction and, in the absence of fluid inertia, is the same as the wave m introduced in § 3.1. The wave q exists because of fluid inertia.

Specifying the unknown constants in a manner similar to § 3.1 furnishes

$$\boldsymbol{F}^X = -4i\pi\omega\rho C_u^{\prime X}\boldsymbol{X}, \quad (3.73)$$

https://doi.org/10.1017/S0022112010005045 Published online by Cambridge University Press

Temperature, T	298 K
Electric field strength, E	25 V cm^{-1}
Particle radius, a	500 nm
Particle dielectric constant, ϵ_p	2.0
Particle density, ρ_p	2000 kg m^{-3}
Water dielectric constant, ϵ_s	78.5
Water viscosity, η	0.89 mPa s
Water density, ρ	997 kg m^{-3}
Brinkman screening length, ℓ	5 nm
Young's modulus, $\mathscr{E}$	1 kPa
Poisson's ratio, ν	0.2
Ionic strength, I	3.78×10^{-3} mol dm^{-3}
fixed-charged density, $\rho^{f\circ}$	1.68×10^4 C m^{-3} ($= 1.05 \times 10^{-4} e$ nm^{-3})
Ion diffusivity, D_s	10^{-9} m^2 s^{-1}
κa	100
βa	10
Da	100
a/ℓ	100
ϵ_p/ϵ_s	0.026

TABLE 1. The principal set of dimensional (upper) and dimensionless (lower) parameters for the results. Note that the ionic strength I includes counterions of the fixed charge and ions from the added salt.

where

$$2\frac{C_u'^E}{a^3} = \rho^{m\circ}\frac{\ell^2}{\eta}\left[\frac{3}{\mathrm{i}}\frac{q^2-(\mathrm{i}\omega/\mu)(\eta/\ell^2)}{s^2-q^2}\frac{\mathrm{i}+q_1a}{q^2a^2} - \frac{3}{\mathrm{i}}\frac{s^2-(\mathrm{i}\omega/\mu)(\eta/\ell^2)}{s^2-q^2}\frac{\mathrm{i}+s_1a}{s^2a^2} + 1\right], \tag{3.74}$$

$$2\frac{C_u'^Z}{a^3} = \mu\frac{\ell^2}{\eta}\frac{3}{i}\left[-s^2\frac{\mathrm{i}+q_1a}{q^2a^2}\frac{q^2-\mathrm{i}(\omega/\mu)(\eta/\ell^2)}{q^2-s^2} + q^2\frac{\mathrm{i}+s_1a}{s^2a^2}\frac{s^2-\mathrm{i}(\omega/\mu)(\eta/\ell^2)}{q^2-s^2}\right] + i\omega. \tag{3.75}$$

Accordingly, the micro-rheological and electrical susceptibilities, now including particle and fluid inertia, are

$$\frac{Z}{F} = \frac{1}{4\mathrm{i}\pi\omega\rho C_u'^Z + 4\pi\omega^2(\rho-\rho_p)a^3/3} \quad \text{and} \quad \frac{Z}{E} = \frac{C_u'^E + \rho^{f\circ}(\ell^2/\eta)a^3/3}{\mathrm{i}\omega(1-\rho_p/\rho)a^3/3 - C_u'^Z}. \tag{3.76}$$

Recall that the micro-rheological susceptibility is independent of the ionic strength and fixed-charge density, because there is no mechanism to perturb the fixed and the mobile charge when the dynamics are incompressible. While the electrical susceptibility is also independent of the ionic strength, it is directly proportional to the fixed-charge density.

4. Results

Below we present the results, using the principal set of parameters listed in table 1, which are representative of the experimental conditions we envision. For clarity, the Brinkman screening length, Young's modulus and Poisson ratio are considered to be independently specified constants. Even though the theory for charged, compressible hydrogels furnishes a good approximation at frequencies less than 1 kHz, we present

https://doi.org/10.1017/S0022112010005045 Published online by Cambridge University Press

results at higher frequencies to (i) compare with the incompressible hydrogel theory and (ii) access the roles of fluid inertia and temporal ion-concentration perturbations.

4.1. *Micro-rheological susceptibility*

In micro-rheology, the forces and the particle displacement are related by $\boldsymbol{Z}(\omega)=\alpha(\omega)\boldsymbol{F}(\omega)$, where $\boldsymbol{Z}(\omega)$, $\boldsymbol{F}(\omega)$ and $\alpha(\omega)$ are, respectively, the particle displacement, applied force and complex susceptibility at angular frequency ω. According to the GSER, the susceptibility for an incompressible linear viscoelastic material is $\alpha(\omega)=[6\pi aG^*(\omega)]^{-1}$, where $G^*(\omega)=G'(\omega)+\mathrm{i}G''(\omega)$ with G' and G'' the storage and loss moduli (Levine & Lubensky 2001). Note that G' and G'' are, in general, frequency-dependent (see Johnson 1982 and the references therein).

We write the susceptibility for a charged viscoelastic material as

$$\alpha(\omega)=\frac{1}{6\pi aG^*(\omega)}Z_F^*(\beta a,\kappa a,a/\ell,\nu,\epsilon_p/\epsilon_s,\omega\eta/\mu,\omega\rho a^2/\eta,\rho_p/\rho), \tag{4.1}$$

where Z_F^* is a dimensionless function of the indicated dimensionless parameters. With incompressible, high-frequency dynamics, Z_F^* is independent of fixed-charge density, ionic strength and particle dielectric constant, i.e. $G^*\to G^*(a/\ell,\omega\eta/\mu,\omega\rho a^2/\eta,\rho_p/\rho)$.

The influence of fixed-charge density is examined in figure 1, where the real and imaginary parts of the susceptibilities Z/F for compressible hydrogels are plotted as a function of ω for various βa. This is achieved by varying the fixed-charge density at constant ionic strength. Also shown are the GSER and the viscoelastic response according to the Stokes formula (Temkin 2005)

$$F/Z=6\pi\eta a(1+a/\delta')\mathrm{i}\omega+(3\pi\rho a^2\delta'+2\pi\rho a^3/3)\omega^2, \tag{4.2}$$

where $\delta'^2=2\eta/(\rho\omega)$. Note that we have replaced the shear viscosity η in (4.2) with $\eta^*=\eta+\mathrm{i}\mu\omega^{-1}$, which, according to viscous–viscoelastic correspondence (Xu, Forest & Klapper 2007), is permissible when the boundary conditions are the same for both media. Thus, the susceptibility from the Stokes formula (4.2) and the result derived in § 3.2 for charged incompressible hydrogels coincide exactly here. This is because the response is independent of electrical charge for incompressible gels, and both results include fluid and particle inertia. As clearly seen in figure 1, incompressible skeletons prevail when $\beta a\gg 1$ because of enhanced electrostatic repulsion between polymers bearing fixed charge (Mohammadi & Hill 2010). Indeed, the low-frequency plateaus in figure 1 are as predicted by Mohammadi & Hill (2010).

To highlight the influence of fixed-charge density on compressional modes, let us briefly consider a charged, compressible hydrogel bounded by a water-permeable solid that oscillates with amplitude $A^{-\mathrm{i}\omega t}$ perpendicular to the interface. This configuration is representative of a compression-stress experiment (Cowin & Doty 2007). Accordingly, (2.3) and (2.4) decouple, giving a displacement that satisfies

$$(\nabla^2-\kappa^2)(\nabla^2+\mathrm{i}\delta^2)\nabla\cdot\boldsymbol{v}'=[\beta^2(1+\nu)(1-2\nu)/(1-\nu)]\nabla^2\nabla\cdot\boldsymbol{v}', \tag{4.3}$$

where δ is given by (3.19). For uncharged hydrogels, this describes the one-dimensional diffusion of $\nabla\cdot\boldsymbol{v}'$ with solution (Landau & Lifshitz 1987)

$$\nabla\cdot\boldsymbol{v}'=(\nabla\cdot\boldsymbol{v}')_{z=0}\ \exp(-z\delta/\sqrt{2})\ \exp[\mathrm{i}(z\delta/\sqrt{2}-\omega t)], \tag{4.4}$$

where z is distance from the interface. Thus, the compressional mode propagates away from the interface and is exponentially damped over a characteristic distance $\sqrt{2}/\delta$. Recall that the associated crossover frequency $\omega_d=D_g/a^2$ is the reciprocal draining

https://doi.org/10.1017/S0022112010005045 Published online by Cambridge University Press

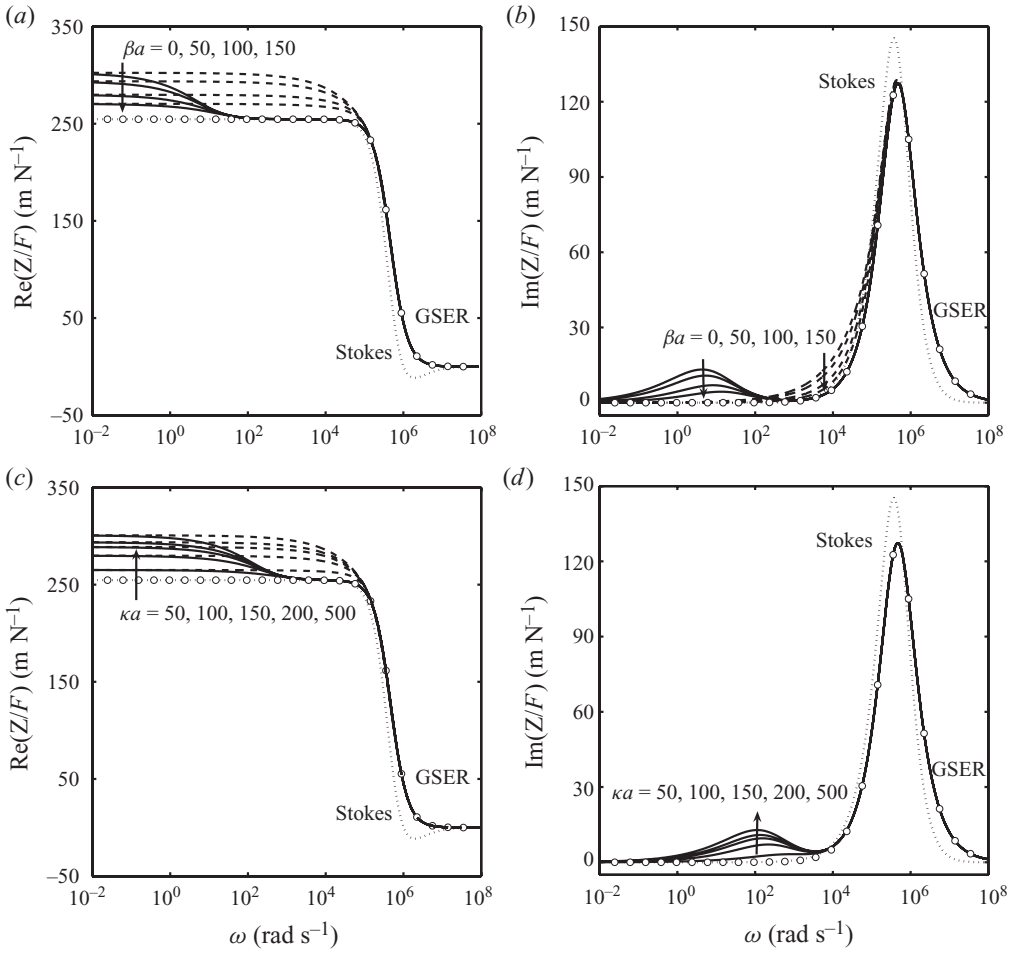


FIGURE 1. The (*a*, *c*) real and (*b*, *d*) imaginary parts of the dynamic susceptibility Z/F versus angular frequency ω. The symbols and the dotted lines are the susceptibility from the GSER (circles) and Stokes formulas (dotted lines). (*a*, *b*) $\kappa a = 100$, $\ell = 1$ and 100 nm (solid and dashed lines, respectively) with several βa; (*c*, *d*) $\beta a = 100$ and $\ell = 5$ nm with several κa. Other parameters are listed in table 1.

time (Levine & Lubensky 2001; Hill & Ostoja-Starzewski 2008), so density modes have finite amplitude when $\omega < \omega_d$.

For charged hydrogels, we have already seen that compressional modes propagate as two longitudinal waves that are exponentially damped over characteristic distances $\sqrt{2\mathrm{i}}/K$ and $\sqrt{2\mathrm{i}}/L$, respectively. The mode with the wavenumber K is an ordinary propagating compressional wave, while the other with the wavenumber L exists because of electrostatic interactions (Epstein & Carhart 1953).

From (3.18), the effective wavenumber associated with the density mode of a charged medium is K, and the corresponding draining frequency is furnished by $\mathrm{Im}(K^2)a^2 = 1$, which retrieves the expected value for an uncharged gel. Electrostatic repulsion among fixed charges on the polymer stiffens the skeleton (Mohammadi & Hill 2010), and the viscous drag between the electrolyte and polymer is dominated by the elastic forces at higher frequencies (see Schnurr *et al.* 1997). Accordingly, the reciprocal draining time for charged gels is smaller than for their uncharged

https://doi.org/10.1017/S0022112010005045 Published online by Cambridge University Press

βa	ω_d (s^{-1})	κa	ω_d (s^{-1})
0	5	50	580
50	6.1	100	240
100	9.5	150	175
150	15.2	200	150
		500	130

TABLE 2. Draining frequencies for the results presented in figure 1 with $\ell = 1$ (left) and 5 (right) nm.

counterparts. This is consistent with the draining frequencies listed in table 2, which are associated with the spectra shown in figure 1.

To our knowledge, the foregoing density modes have not been observed in micro-rheology (MacKintosh & Levine 2008), although Tanaka *et al.* (1973, 1977) detected them in polyacrylamide hydrogels, using light scattering. Our theory quantifies how electrostatic repulsion among fixed charges attenuates density modes, suggesting that their experimental observation is elusive because most subjects of micro-rheology bear fixed charge; e.g. F-actin and neutral polymers such as polyacrylamide become charged because of hydrolysis.

Other characteristic frequencies are ω^* (corresponding to the wavenumber q) and ω_v (corresponding to the wavenumber m or s). The first, adopted by Levine and Lubensky (2000, 2001) – from the Fourier transform of their two-fluid model – is indicative of fluid inertia, and the second, introduced and measured by Tanaka *et al.* (1973), corresponds to the propagation of a transverse wave associated with viscous friction between the fluid and the polymer skeleton.

The susceptibility predicted by our model for charged compressible hydrogels coincides with the GSER at high frequencies. However, both theories neglect fluid and particle inertia, so they both depart from the Stokes formula at high frequencies. Since both the Stokes formula and the GSER are for incompressible media, they coincide at low frequencies. Accordingly, the GSER and Stokes formulas provide the correct asymptotic limit of our model for highly charged or intrinsically incompressible polymer skeletons when inertial influences are negligible.

Generally, the influences of fixed charge and ionic strength on the susceptibility are small compared with, for example, boundary conditions that permit polymer slip at the particle surface (Fu *et al.* 2008). Polymer-displacement boundary conditions affect only the low-frequency response, whereas fluid-slip boundary conditions become important at high frequencies. Note that the influence of fixed charge and ionic strength on the susceptibility cannot be replicated by introducing empirically modified compressibility parameters. Electrostatic interactions in micro-rheological experiments perturb the equilibrium state of material under study. The present theory examines the influence of the perturbations to equilibrium viscoelastic properties. If parameters are modified empirically, they account only for the equilibrium state, not the perturbations induced by a micro-rheology experiment or, indeed, during an experiment in which the polymer skeleton undergoes compression and dilation.

4.2. *Electrical susceptibility*

The electrical susceptibility can be written:

$$Z/E = -\rho^{f\circ}\ell^2(i\omega\eta - \mu)^{-1}Z_E^*(\beta a, \kappa a, a/\ell, \nu, \epsilon_p/\epsilon_s, \omega\eta/\mu, \omega\rho a^2/\eta, \rho_p/\rho), \qquad (4.5)$$

https://doi.org/10.1017/S0022112010005045 Published online by Cambridge University Press

where Z_E^* is a dimensionless function of the indicated dimensionless parameters. The characteristic frequencies associated with the response are the same as for the Z-problem. In contrast to the foregoing micro-rheological susceptibility Z/F, the electrical susceptibility directly reflects the fixed-charge density.

For incompressible hydrogels, however, the electrical susceptibility is independent of the ionic strength and particle dielectric constant. Following Mohammadi & Hill (2010) for the steady response, the quasi-steady electrical response for incompressible hydrogels without fluid or particle inertia is simply

$$Z/E = \rho^{f\circ}\ell^2(\mathrm{i}\omega\eta - \mu)^{-1} \quad \text{for} \quad \nu = 0.5. \tag{4.6}$$

This results from adding the quasi-steady equations of motion for the Newtonian fluid and the incompressible elastic solid, giving $0 = -\nabla p' + \nabla^2 \boldsymbol{w}'$ and $\nabla \cdot \boldsymbol{w}' = 0$, where $\boldsymbol{w}' = \eta \boldsymbol{u}' + \mu \boldsymbol{v}'$. Note that $-p'\boldsymbol{I}$ and $(1/2)[\nabla \boldsymbol{w}' + (\nabla \boldsymbol{w}')^{\mathrm{T}}]$ are, respectively, the isotropic and deviatoric stresses for an incompressible viscoelastic continuum. The E-problem has boundary conditions $\boldsymbol{w}' \to -\rho^{f\circ}(\ell^2/\eta)\boldsymbol{E}$ as $r \to \infty$ and $\boldsymbol{w}' = 0$ at $r = a$. Accordingly, the force in the E-problem is the same as the hydrodynamic force for a Newtonian Stokes flow, but with far-field velocity $-\rho^{f\circ}(\ell^2/\eta)\boldsymbol{E}$, giving $\boldsymbol{F}^E = -6\pi a \ell^2 \rho^{f\circ}\boldsymbol{E}$. The force in the Z-problem is, again, the Stokes drag force with complex shear viscosity $\eta^* = \eta + \mathrm{i}\mu\omega^{-1}$ replacing the Newtonain shear viscosity η. Thus, $\boldsymbol{F}^Z = -6\pi a(\mu - \mathrm{i}\omega\eta)\boldsymbol{Z}$, and (4.6) is recovered.

The effects of fixed-charge density on the real and imaginary parts of the electrical susceptibility are shown in figure 2(a, b). The theory for compressible hydrogels (solid lines) is compared with (4.6) for an incompressible hydrogel with the same shear modulus. Recall that neither theory includes particle or fluid inertia, so the close correspondence at high frequencies merely confirms that the compressible hydrogels behave as incompressible hydrogels at frequencies above the reciprocal draining time. Note that the transition from compressible to incompressible dynamics increases with the fixed-charge density in the same manner as the Z-problem. Moreover, in contrast to the micro-rheological susceptibility, high-frequency electrical response depends on the fixed-charge density, as indicated by (4.5) and (4.6).

The influences of ionic strength on the electrical susceptibility are shown in figure 2(c, d), again for compressible (solid lines) and incompressible (dashed lines) hydrogels. Note that the response at low frequencies increases with the ionic strength, since the electrolyte screens the electrostatic repulsion among fixed charges and, therefore, increases dilatational strain. Softening of intrinsically compressible hydrogels with increasing ionic strength vanishes when $\omega \gg \omega_d$ because, similar to the Z-problem (figure 1), hydrodynamic coupling of the skeleton with the incompressible fluid prevents dilatational strain.

To examine the influences of fluid and particle inertia, figure 3 compares the theory for compressible hydrogels (without inertia and ion-concentration perturbations) (solid lines; (3.48)) with the theory for incompressible hydrogels, which includes inertia and ion-concentration perturbations (dashed lines; (3.76)). As expected from the analysis of time scales, fluid and particle inertia manifest at high frequencies ($\gtrsim 10^5$ Hz). At low frequencies, the steady asymptotes agree with Mohammadi & Hill (2010) (dash-dotted lines). Note that inertial contributions to the response are significant under conditions where displacements are extraordinarily small. This motivates the following examination of the dynamic mobility, which is the fundamental quantity used to interpret electro-acoustic experiment performed in the ultrasonic (megahertz) frequency range.

https://doi.org/10.1017/S0022112010005045 Published online by Cambridge University Press

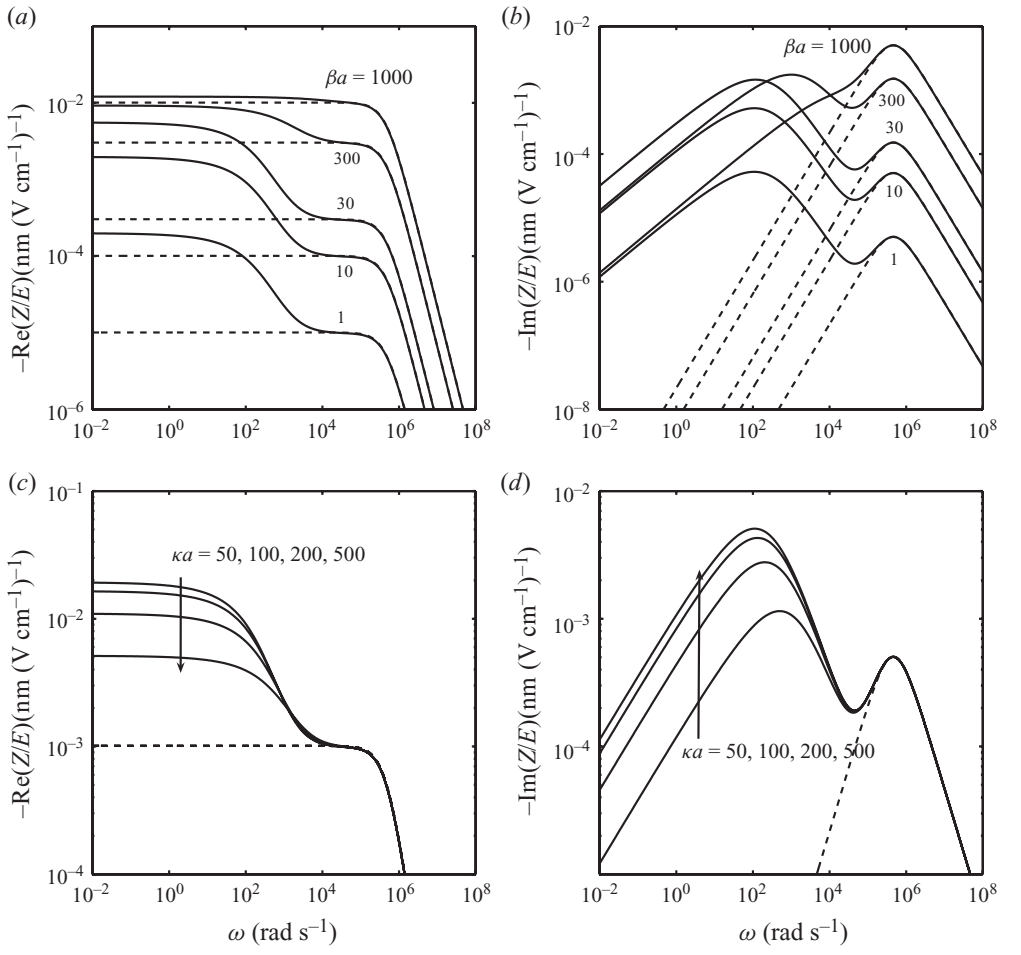


FIGURE 2. The (*a*, *c*) real and (*b*, *d*) imaginary parts of the electrical susceptibility Z/E versus angular frequency ω: (*a*, *b*) $\kappa a = 100$ with $\beta a = 1$, 10, 100 and 1000; and (*c*, *d*) $\beta a = 100$ with $\kappa a = 50$, 100, 200 and 500. Other parameters are listed in table 1. The solid lines are our electrokinetic model for charged, compressible hydrogels without inertia and temporal ion-concentration perturbations; and the dashed lines are from (4.6) for incompressible hydrogels, also without inertia and ion-concentration perturbations.

4.3. *Harmonic-oscillator model*

Before addressing the electro-acoustic response, we briefly digress to present a phenomenological theory that addresses – in an approximate manner – the dynamics of a charged inclusion embedded in a charged hydrogel. The inclusion is modelled as an harmonic oscillator with position $Ze^{-i\omega t}$ that satisfies the equation of motion

$$-\omega^2 \rho_p V_p Z = i\omega\alpha_1 6\pi\eta^* a Z - \alpha_2 6\pi\rho^{f\circ} a\ell^2 E + \alpha_3 4\pi\sigma a^2 E, \tag{4.7}$$

where the dimensionless pre-factors

$$\alpha_1 = 1 - (i-1)\sqrt{\delta^*} - 2i\delta^*/9 \quad \text{and} \quad \alpha_2 = 1 - i\sqrt{\alpha'} - \alpha'/3 \tag{4.8}$$

with $\alpha' = ia^2\omega\rho/\eta$, $\eta^* = \eta + i\mu\omega^{-1}$ and $\delta^* = \rho\omega a^2/(2\eta^*)$. The left-hand side of (4.7) is the particle inertia, and the terms on the right-hand side are, respectively, a viscoelastic restoring force, an electro-osmotic drag force and an electrical force (proportional

https://doi.org/10.1017/S0022112010005045 Published online by Cambridge University Press

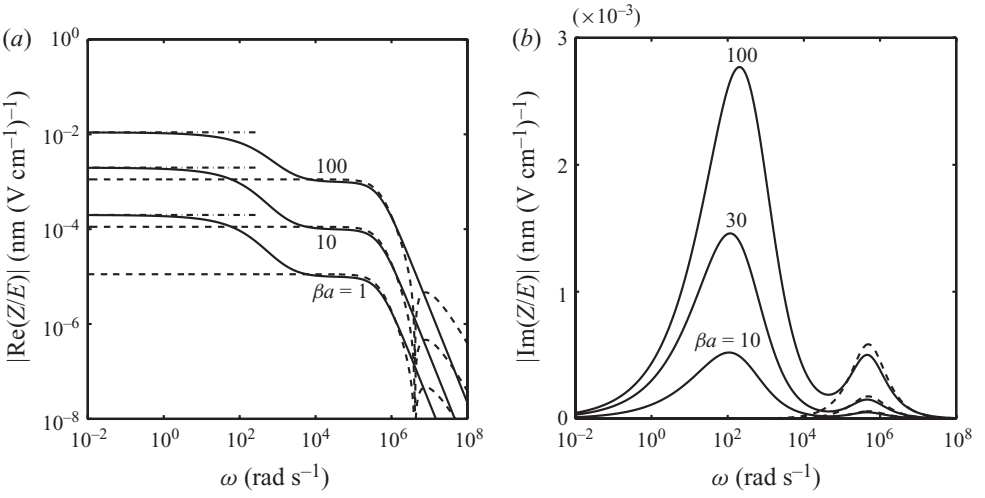


FIGURE 3. The (*a*) real and (*b*) imaginary parts of the electrical susceptibility Z/E versus angular frequency ω: $\kappa a = 100$ with various βa. Other parameters are listed in table 1. The solid lines are our electrokinetic model for charged, compressible hydrogels without inertial influences and temporal ion-concentration perturbations (3.48); the dashed lines are the response for incompressible hydrogels (3.76) with inertia and ion-concentration perturbations; and the dash-dotted lines are steady asymptotes from Mohammadi & Hill (2010).

to the bare Coulomb force). Here, $V_p = (4/3)\pi a^3$ is the particle volume, and σ is the particle surface charge density. Note that we have applied viscous–viscoelastic correspondence to evaluate α_1, using the Stokes formula (4.2), and the expression for α_2 is an approximation from our full theory that is valid when $\omega \gg \mu/\eta$. Finally, α_3 is a dimensionless function that corrects the bare Coulomb electrical force for diffuse-double-layer screening and dynamics.

According to (4.7), the electrical susceptibility is

$$\frac{Z}{E} = \frac{\alpha_2 6\pi\rho^{f\circ} a\ell^2 - \alpha_3 4\pi\sigma a^2}{\alpha_1 6\pi\eta^* a i\omega + \rho_p V_p \omega^2}, \tag{4.9}$$

which demonstrates, at least qualitatively, how the particle and polyelectrolyte charge each contribute to the particle dynamics. Obviously, setting $\sigma = 0$ furnishes an approximate model that captures the essential physics of our more rigorous model when $\omega \gg \mu/\eta$. Note that the ratio of the hydrogel and particle contributions to the electrical forcing is

$$\frac{\alpha_2}{\alpha_3}\frac{3\rho^{f\circ}\ell^2}{2\sigma a}, \tag{4.10}$$

so, for example, with $\sigma \sim -1\,\mu\mathrm{C\,cm^{-2}}$ and the other parameters listed in table 1, the ratio is $\sim -10^{-3}\alpha_2/\alpha_3$. Therefore, for quasi-steady dynamics where $\alpha_2 \sim \alpha_3 \sim 1$, the hydrogel charge contribution would be small. Note that α_3 can vary with a/ℓ and κa, among several other dimensionless parameters. Thus, more specific conclusions demand consideration of specific system parameters, as we have undertaken for uncharged particles in charged hydrogels and as Wang & Hill (2008) considered for charged particles in uncharged gels.

At asymptotically low frequencies,

$$Z/E \to (2/3)\alpha_3\sigma a/\mu - \rho^{f\circ}\ell^2/\mu, \tag{4.11}$$

https://doi.org/10.1017/S0022112010005045 Published online by Cambridge University Press

showing that the response of an uncharged particle in a charged hydrogel is independent of the particle size and fluid viscosity. Moreover, a like-signed charge on the particle and gel produces a displacement that can be positive or negative, depending on the particle size and charge, and polyelectrolyte charge and hydrodynamic permeability.

At asymptotically high frequencies,

$$Z/E \to -\sigma\,[6\alpha_3/(\rho_p a\omega^2)]/(2+\rho_p/\rho) - 3\mathrm{i}\omega^{-1}\rho^{f\circ}(\ell^2/\eta)(\rho/\rho_p)/(2+\rho/\rho_p), \qquad (4.12)$$

showing that the hydrogel charge dominates the particle dynamics at high frequencies.

Finally, the harmonic oscillator can be modified to yield a dynamic electrophoretic mobility

$$\mu_E = \frac{U}{E} + \frac{\rho^{f\circ}\ell^2}{\eta}\,\frac{\alpha_1 6\pi\eta^* a\mathrm{i}\omega + \rho V_p\omega^2}{\alpha_1 6\pi\eta^* a\mathrm{i}\omega + \rho_p V_p\omega^2}, \qquad (4.13)$$

where $U/E = -\mathrm{i}\omega Z/E$ and Z/E is given by (4.9). At asymptotically low frequencies, $\mu_E \to \rho^{f\circ}\ell^2/\eta$, and at asymptotically high frequencies, $\mu_E \to 0$. Quantitative comparisons of this model with the full model for uncharged particles in charged hydrogels are undertaken below.

4.4. *Electro-acoustic response and dynamic electrophoretic mobility*

An electro-acoustic response (O'Brien 1988; Wang & Hill 2009) is conventionally considered to arise from electrical charge on colloidal particles dispersed in Newtonian electrolytes. It includes the generation of an electric field by a sound wave, and vice versa. When a sound wave passes through a colloidal dispersion, relative motion of the particles and surrounding fluid induces an alternating charge polarization that produces an electric field that can be measured and related to microscopic properties of the dispersion. Conversely, when an oscillating electric field is applied, collective electrophoretic particle motion produces acoustic pressure fluctuations, which can be measured and, again, related to microscopic properties.

By generalizing the electro-acoustic effects for colloidal dispersions pioneered by O'Brien (1988, 1990), Wang & Hill (2009) theoretically analysed electro-acoustics of hydrogel-colloid composites, showing how these depend on viscoelastic properties of the gel. Their work is limited to uncharged hydrogels and, similarly, to colloidal dispersions and emulsions, electro-acoustic effects arise from charge on the inclusions. Recall that most biological and many synthetic hydrogels bear fixed charge, so to isolate the effects arising from charge on the particle from charge on the hydrogel, we restrict the following analysis to uncharged colloidal inclusions embedded in charged polymer skeletons. Here, the response arises from the propagation of coupled electrical and mechanical waves and the delayed response of the particles relative to the surrounding medium. Similar waves are produced in saturated, charged porous media (Pride 1994). Note that waves due to ion–fluid coupling are beyond the scope of this study but are generally removed experimentally by subtracting the electro-acoustic response without inclusions. Similar practical issues are encountered when measuring the colloid vibration potential and the electrokinetic sonic amplitude of particles dispersed in Newtonian fluids (Desai, Hammad & Hayes 1993; Hunter 1998).

To calculate the electro-acoustic response, we proceed by establishing the link between microscopic characteristics and the macro-scale dynamics. Following O'Brien

https://doi.org/10.1017/S0022112010005045 Published online by Cambridge University Press

(1988), the relevant equations in the particle-fixed reference frame are

$$-\epsilon_o\epsilon_s\nabla^2\psi' = \sum_j n_j' z_j \mathrm{e} + \rho^{f\prime}, \tag{4.14}$$

$$\mathrm{i}\omega n_j' = -D_j\nabla\cdot\left(\nabla n_j' + n_j^\circ\frac{z_j\mathrm{e}}{k_BT}\nabla\psi' + n_j'\frac{z_j\mathrm{e}}{k_BT}\nabla\psi^\circ\right) + \nabla n_j^\circ\cdot\boldsymbol{u}', \tag{4.15}$$

$$-\mathrm{i}\omega\rho^\circ(\boldsymbol{u}'+\boldsymbol{U}) = \nabla\cdot\boldsymbol{\sigma}^h - \sum_j z_j\mathrm{e}(n_j^\circ\nabla\psi' + n_j'\nabla\psi^\circ) - \frac{\eta}{\ell^2}(\boldsymbol{u}'+\mathrm{i}\omega\boldsymbol{v}'), \tag{4.16}$$

$$0 = -\nabla\cdot\boldsymbol{\sigma}^{\mathrm{e}} - \frac{\eta}{\ell^2}(\boldsymbol{u}'+\mathrm{i}\omega\boldsymbol{v}') + \rho^{f\circ}\nabla\psi' + \rho^{f\prime}\nabla\psi^\circ, \tag{4.17}$$

$$0 = \nabla\cdot\boldsymbol{u}', \tag{4.18}$$

$$\rho^{f\prime} = -\rho^{f\circ}\nabla\cdot\boldsymbol{v}' - \nabla\rho^{f\circ}\cdot\boldsymbol{v}', \tag{4.19}$$

where $\boldsymbol{U}$ is the particle velocity. Note that the fluid is considered incompressible when the sound wavelength is much greater than the characteristic microscopic length scale set by the particle radius (O'Brien 1988). The foregoing equations are applicable to the more general case of a charged colloidal inclusion in a charged hydrogel; for the uncharged particles in this work, recall that $\rho^{f\circ}=$ constant and $\psi^\circ=0$.

The average particle velocity $\langle\boldsymbol{U}\rangle$ and the average current density $\langle\boldsymbol{i}\rangle$ are required to calculate the electro-acoustic response. These are related to the average electric field $\langle\boldsymbol{E}\rangle$ and the average pressure gradient $\nabla\langle p\rangle$ by

$$\langle\boldsymbol{i}\rangle = L\nabla\langle p\rangle + K^*\langle\boldsymbol{E}\rangle, \tag{4.20}$$

$$\langle\boldsymbol{U}\rangle = \alpha\nabla\langle p\rangle + \mu_E\langle\boldsymbol{E}\rangle, \tag{4.21}$$

where K^* and μ_E are, respectively, the complex conductivity and the particle (dynamic) electrophoretic mobility (O'Brien 1988). Here, L (not to be confused with the wavenumber above) is adopted in place of O'Brien's β.

Note that the foregoing relationships define μ_E as the ratio of the average particle velocity to the average electric field strength, in the absence of an average pressure gradient. Thus, μ_E should be calculated theoretically at finite frequencies with zero far-field fluid velocity when the skeleton has negligible inertia. This demands a far-field boundary condition where the charged skeleton translates through a quiescent electrolyte, since the electrical force on the skeleton is balanced by its hydrodynamic coupling with the electrolyte, which is balanced by the electrical force on the mobile countercharge.

In contrast to colloidal dispersions and hydrogel-colloid composites with uncharged polymer, the electrical current density in charged hydrogels includes the flux of fixed charge. Accordingly, the current density

$$\boldsymbol{i} = \sum_j \boldsymbol{j}_j z_j\mathrm{e} - \mathrm{i}\omega\rho^{f\circ}\boldsymbol{v}' + \mathrm{i}\omega\epsilon_o\epsilon_s\nabla\psi', \tag{4.22}$$

where first and second terms on the right-hand side account for the flux of mobile and fixed ions, respectively, and the third term includes polarization of the dielectric medium (O'Brien 1982). Note that factors $\mathrm{e}^{-\mathrm{i}\omega t}$ are implicitly implied for all perturbed quantities. From the Poisson equation and the fixed-charge and mobile-ion conservation equations, $\nabla\cdot\boldsymbol{i}=0$.

O'Brien (1988) has shown that only L and μ_E are required to interpret general electro-acoustic responses, i.e. the colloid vibration potential and the electrokinetic sonic amplitude, and furthermore, he showed that these are related by a reciprocal

https://doi.org/10.1017/S0022112010005045 Published online by Cambridge University Press

identity. Following O'Brien (1988, 1990) and Wang & Hill (2009), the reciprocal identity is furnished by evaluating the following integral involving two solutions of the governing equations, denoted by the superscripts a and b, for different macroscopic quantities:

$$\frac{1}{V}\int_A \left[\boldsymbol{u}'^a\cdot(\boldsymbol{\sigma}^{hb}+\mathrm{i}\omega\rho\boldsymbol{U}^b\boldsymbol{x}\cdot\boldsymbol{I})-\mathrm{i}\omega\boldsymbol{v}'^a\cdot\boldsymbol{\sigma}^{eb}-\boldsymbol{i}^a\psi'^b-\sum_j\frac{k_BT}{n_j^\circ}n_j'^b\left(\boldsymbol{j}_j^a-n_j^\circ\boldsymbol{u}'^a\right)\right]\cdot\hat{\boldsymbol{n}}\,\mathrm{d}A. \tag{4.23}$$

This integral can be shown to be symmetric with respect to exchange of a and b (see O'Brien 1988, 1990; Wang & Hill 2009), giving

$$-\langle\boldsymbol{u}'\rangle^a\cdot[\nabla\langle p\rangle^b-\mathrm{i}\omega\rho\langle\boldsymbol{U}\rangle^b]+\langle\boldsymbol{i}\rangle^a\cdot\langle\boldsymbol{E}\rangle^b, \tag{4.24}$$

which is the same result as O'Brien (1988, 1990) and Wang & Hill (2009). Since this is symmetric with respect to exchange of a and b, if $\nabla\langle p\rangle^a=\langle\boldsymbol{E}\rangle^b=0$, then

$$-\langle\boldsymbol{u}'\rangle^a\cdot[\nabla\langle p\rangle^b-\mathrm{i}\omega\rho\langle\boldsymbol{U}\rangle^b]=\mathrm{i}\omega\rho\langle\boldsymbol{U}\rangle^a\cdot\langle\boldsymbol{u}'\rangle^b+\langle\boldsymbol{i}\rangle^b\cdot\langle\boldsymbol{E}\rangle^a. \tag{4.25}$$

Thus, because the total force on the volume V enclosed by the surface A vanishes as $V\to\infty$, we find

$$-\nabla\langle p\rangle=-\mathrm{i}\omega\rho(\langle\boldsymbol{u}'\rangle+\langle\boldsymbol{U}\rangle)-\mathrm{i}\omega\phi(\rho_p-\rho)\langle\boldsymbol{U}\rangle. \tag{4.26}$$

Finally, with (4.25), the reciprocal identity is

$$L=\phi\mu_E(\rho_p-\rho)/\rho, \tag{4.27}$$

where $\phi\ll1$ is the inclusion volume fraction. Accordingly, the electro-acoustic response is the same as O'Brien's formula for colloidal dispersions. As shown in Appendix A, however, the requisite dynamic electrophoretic mobility

$$\mu_E=\frac{-\mathrm{i}\omega f^E-f^Z(\ell^2/\eta)\rho^{f\circ}}{(\rho-\rho_p)V_p\omega^2-f^Z}. \tag{4.28}$$

Note that this quantity is qualitatively different from $U/E=-\mathrm{i}\omega Z/E$ with Z/E given by (3.5). The difference, which is examined below, does not exist for charged particles dispersed in Newtonian electrolytes or uncharged hydrogels when $\phi\ll1$, because the bulk medium in these problems bears only an $O(\phi)$ fixed-charge density. For concentrated dispersions, however, it is well known that the dynamic electrophoretic mobility must be calculated in the zero-momentum reference frame (Ahualli *et al.* 2007).

Dynamic mobility spectra are shown in figure 4 for several fixed-charge densities and a constant Young's modulus. Recall that dilatation is suppressed by coupling with the incompressible fluid at these high frequencies. The dynamic mobility U/E in figure 4(*a*,*b*) monotonically increases with the fixed charge and, generally, has a large amplitude compared with the values for charged inclusions in uncharged hydrogels (Wang & Hill 2009). For example, with the parameters listed in table 1, the mobility is $\sim4\,\mu\mathrm{m\,s^{-1}}\ (\mathrm{V\,cm^{-1}})^{-1}$ for an inclusion with surface potential $\zeta\sim-2k_BT/\mathrm{e}$ in an uncharged gel (see Wang & Hill 2009). In figure 4(*a*, *b*), however, $U/E\sim10\,\mu\mathrm{m\,s^{-1}}\ (\mathrm{V\,cm^{-1}})^{-1}$, even though the particle is uncharged. Noteworthy is that the vanishing low-frequency mobility rapidly transits to the high-frequency plateau at a frequency that is reciprocal to the $\sim\eta/\mu=\eta3/\mathscr{E}^\circ$ viscoelastic time scale. Moreover, the high-frequency plateau reflects the hydrogel charge and permeability, with a weak dependence on the elastic modulus and particle size. In striking contrast,

https://doi.org/10.1017/S0022112010005045 Published online by Cambridge University Press

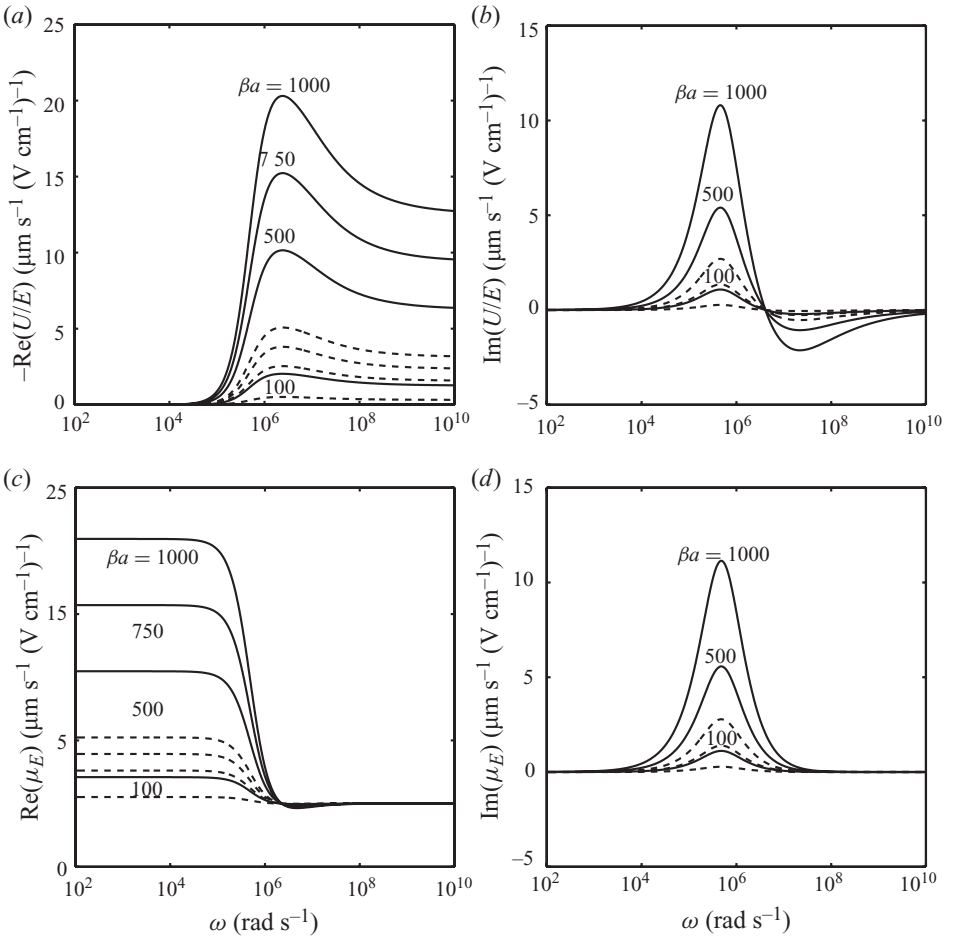


FIGURE 4. The (*a*, *c*) real and (*b*, *d*) imaginary parts of the dynamic mobilities (*a*, *b*) U/E (defined with zero far-field polymer displacement) and (*c*, *d*) μ_E (defined with zero far-field pressure gradient) versus angular frequency ω: $\ell = 5$ and 10 nm (dashed and solid lines, respectively) with various values of βa and other parameters listed in table 1.

the dynamic electrophoretic mobility μ_E shown in figure 4(*c*, *d*) has a finite low-frequency plateau, which, from inspection of (4.28), is the electro-osmotic flow mobility $(\ell^2/\eta)\rho^{f\circ}$. Clearly, under conditions with zero far-field pressure gradient and, thus, vanishing far-field fluid velocity, the particle translates in unison with the undisturbed polymer skeleton. At $\sim\mu/\eta$ frequencies, however, the particle dynamics in the skeleton reference frame become comparable to the bulk electro-osmotic flow, so at higher frequencies the two oppositely directed velocities eventually cancel. Instead of a dynamic mobility that increases with frequency in the transition regime, μ_E rapidly decreases.

Dynamic electrohporetic mobility spectra are shown in figure 5 for several values of Young's modulus with Brinkman screening lengths $\ell = 5$ and 10 nm (dashed and solid lines, respectively). Here, the fixed-charge density $\rho^{f\circ} = 10^6\,\mathrm{C\,m^{-3}}$ is an order of magnitude smaller than the maximum value set by Manning counterion condensation (Mohammadi & Hill 2010). Again, the transitions from high- to low-frequency dynamics reflect the characteristic viscoelastic and inertial time scales. Thus, while the mobility amplitude increases with decreasing elastic modulus and increasing

https://doi.org/10.1017/S0022112010005045 Published online by Cambridge University Press

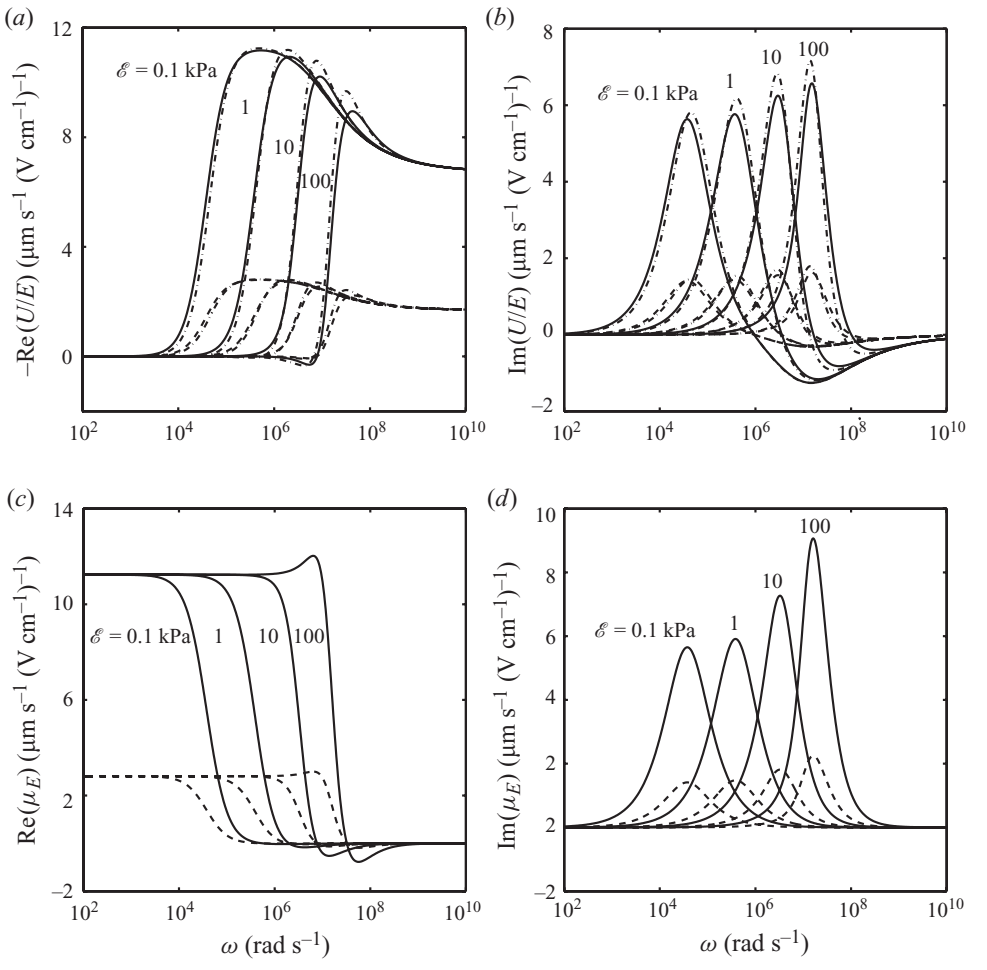


FIGURE 5. The (*a*, *c*) real and (*b*, *d*) imaginary parts of the dynamic mobilities (*a*, *b*) U/E (defined with zero far-field polymer displacement) and (*c*, *d*) μ_E (defined with zero far-field pressure gradient) versus angular frequency ω: $\ell = 5$ and 10 nm (dashed and solid lines, respectively) with various Young's moduli $\mathscr{E}$, fixed-charge density $\rho^{f\circ} = 10^6\,\mathrm{C\,m^{-3}}$ and other parameters listed in table 1. The dash-dotted lines in (*a*) and (*b*) are the harmonic-oscillator model (4.9).

fixed-charge density and hydrodynamic permeability, the characteristic frequencies reflect the elastic modulus and particle size, as expected from the functional form of the wavenumbers q and s. Note that because the inclusions are uncharged, and the dilatational modes are absent, the electric-field-induced dynamics are independent of the ionic strength. As expected, the characteristic frequencies are practically independent of the permeability, but the mobility amplitude has a clear quadratic dependence on ℓ, because the bulk electro-osmotic flow is proportional to ℓ^2. The dash-dotted lines in figure 5(*a*, *b*) are from the harmonic-oscillator model (4.9). Clearly, this furnishes a convenient and reasonably accurate approximation of U/E from the full model.

Dynamic mobility spectra are shown in figure 6 for several values of Young's modulus, but with particle radii $a = 0.5$ and 5 μm (dashed and dotted lines, respectively). Again, the fixed-charge density $\rho^{f\circ} = 10^6\,\mathrm{C\,m^{-3}}$. At lower frequencies, the mobilities U/E and μ_E are both practically independent of particle size, because

https://doi.org/10.1017/S0022112010005045 Published online by Cambridge University Press

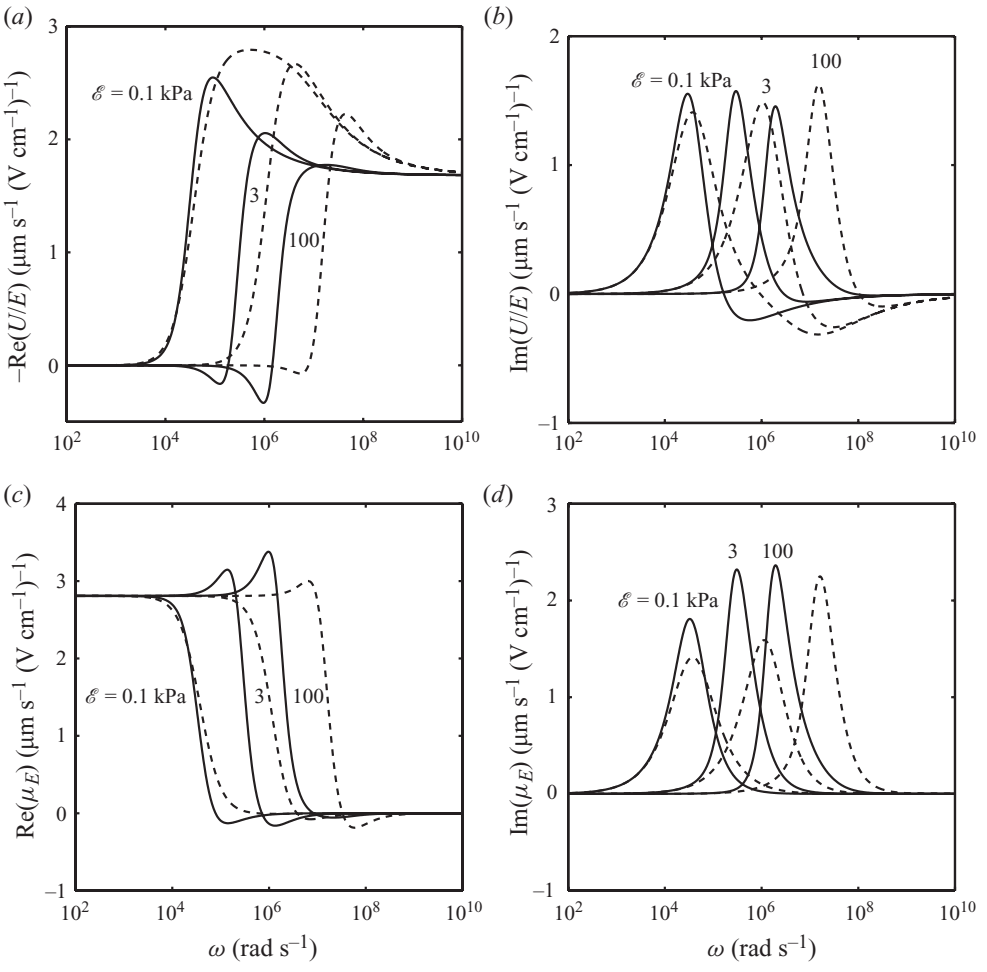


FIGURE 6. The (*a*, *c*) real and (*b*, *d*) imaginary parts of the dynamic electrophoretic mobilities (*a*, *b*) U/E (defined with zero far-field polymer displacement) and (*c*, *d*) μ_E (defined with zero far-field pressure gradient) versus angular frequency ω: $a = 0.5$ and 5 μm (dashed and solid lines, respectively) with various Young's moduli $\mathscr{E}$, fixed-charge density $\rho^{f\circ} = 10^6\,\mathrm{C\,m^{-3}}$ and other parameters listed in table 1.

inertial forces are weak compared with the electrical and viscous forces. This is similar to the response of charged colloidal particles in Newtonian electrolytes (see Hunter 1998). At higher frequencies, however, inertia causes the particle dynamics to lag the applied field, so the mobility depends on the particle size at moderately high frequencies, shifting the transition from the low- to high-frequency plateaus to higher frequencies. Interestingly, at asymptotically high frequencies, the influence of particle size vanishes again, because the dynamic mobility reflects a balance of inertial forces that both scale with the particle volume. Generally, particle size has a very weak influence on the mobility as compared with the hydrogel permeability. Increasing the particle size increases both the drag and restoring forces, which scale as a^n with $2 < n < 3$ (see (3.74)–(3.76)), so U/E does indeed have a weak dependence on particle size, scaling as a^m with $0 < m < 1$.

https://doi.org/10.1017/S0022112010005045 Published online by Cambridge University Press

5. Summary

We calculated the dynamic electrical response of an uncharged micro-sphere embedded in a quenched polyelectrolyte hydrogel. The polyelectrolyte was modelled as a three-component fluid, including dynamical terms previously neglected in the calculation of the steady response by Mohammadi & Hill (2010). To furnish analytical solutions, we addressed two simplified problems: one for compressible skeletons without fluid inertia and ion-concentration perturbations and another for incompressible skeletons with particle and fluid inertia and ion-concentration perturbations. The former model captures the coupling of hydrodynamic draining and electrostatics at low frequencies, while the latter captures the dynamics at frequencies above the reciprocal draining time of compressible polymer gels.

First, we calculated how the micro-rheological susceptibility Z/F transits between the limits for uncharged, compressible media and intrinsically incompressible viscoelastic media when increasing the fixed-charge density or decreasing the ionic strength. This is analogous to the steady susceptibility calculated by Mohammadi & Hill (2010). With increasing frequency, however, these influences vanish because of hydrodynamic coupling with the incompressible electrolyte.

Next, we examined how the electrical susceptibility Z/E depends on the fixed-charge density and ionic strength through coupling of the electrostatics with the hydrodynamic and compressible elastic modes. At high frequencies, the influence of ionic strength vanishes, and the three-phase fluid behaves as a single incompressible, viscoelastic medium. Note, however, that the fixed-charge density plays an important role at all frequencies: at low frequencies it affects the driving (electro-osmotic) and restoring (compressible, elastic) forces, whereas at high frequencies it only affects the driving force.

Finally, we studied how the electrical susceptibility is related to the electrokinetic sonic amplitude, which is measured in commercial instruments at ultrasonic frequencies. The electrokinetic sonic amplitude is proportional to the dynamic electrophoretic mobility μ_E in the zero-momentum reference frame. For uncharged inclusions in charged hydrogels, the dynamic mobility is large compared with the response of charged inclusions in uncharged hydrogels, previously calculated by Wang & Hill (2009). Interestingly, μ_E is finite at low frequencies – reflecting only the intrinsic hydrogel electro-osmotic flow mobility – and vanishes at asymptotically high frequencies. The transition from the low- to high-frequency regimes principally reflects the characteristic viscoelastic time scale and, hence, the hydrogel dynamic shear modulus.

R.J.H. gratefully acknowledges support from the Natural Sciences and Engineering Research Council of Canada and the Canada Research Chairs programme. A.M. thanks the McGill Faculty of Engineering for generous financial support through a McGill Engineering Doctoral Award.

Appendix A. Boundary conditions and equation of motion for electric-field-induced particle dynamics

The boundary conditions satisfied by superposing the solutions of the Z-problem and the E-problem solved in the main text are

$$\boldsymbol{v}' = \boldsymbol{u}' = 0 \quad \text{at} \quad r = a, \tag{A 1}$$

$$\boldsymbol{v}' \to -\boldsymbol{Z}' \quad \text{and} \quad \boldsymbol{u}' \to \mathrm{i}\omega\boldsymbol{Z}' - (\ell^2/\eta)\rho^{f\circ}\boldsymbol{E} \quad \text{as} \quad r \to \infty \tag{A 2}$$

https://doi.org/10.1017/S0022112010005045 Published online by Cambridge University Press

and

$$\nabla p' \to -\rho\omega^2 \boldsymbol{Z}' - \mathrm{i}\omega\rho(\ell^2/\eta)\rho^{f\circ}\boldsymbol{E} \text{ as } r \to \infty. \tag{A 3}$$

Recall that these produce a force $f^Z\boldsymbol{Z}' + f^E\boldsymbol{E}$ on the stationary particle. Note that $\boldsymbol{Z}'$ here denotes the displacement of the skeleton relative to the fixed particle.

To have a far-field pressure gradient that vanishes upon superposition to satisfy the particle equation of motion, we must have

$$\mathrm{i}\omega\boldsymbol{Z}' = \mathrm{i}\omega\boldsymbol{Z} + (\ell^2/\eta)\rho^{f\circ}\boldsymbol{E}. \tag{A 4}$$

Accordingly, superposing all the forces (from the rigid-body translation and the disturbances in the Z-problem and the E-problem) yields an equation of motion

$$-\rho_p V_p \omega^2 \boldsymbol{Z} = -\rho V_p \omega^2 \boldsymbol{Z} + f^Z[\boldsymbol{Z} + (\ell^2/\eta)\rho^{f\circ}\boldsymbol{E}/(\mathrm{i}\omega)] + f^E\boldsymbol{E}, \tag{A 5}$$

so

$$\frac{Z}{E} = \frac{f^E + f^Z(\ell^2/\eta)\rho^{f\circ}/(i\omega)}{(\rho - \rho_p)V_p\omega^2 - f^Z}. \tag{A 6}$$

Note that the boundary conditions in the laboratory reference frame are

$$\boldsymbol{v}' = \boldsymbol{Z} \quad \text{and} \quad \boldsymbol{u}' = -\mathrm{i}\omega\boldsymbol{Z} \quad \text{at} \quad r = a, \tag{A 7}$$

$$\boldsymbol{v}' \to 0 \quad \text{and} \quad \boldsymbol{u}' \to 0 \quad \text{as} \quad r \to \infty \tag{A 8}$$

and

$$\nabla p' \to 0 \quad \text{as} \quad r \to \infty. \tag{A 9}$$

These yield a particle velocity at zero frequency where the skeleton and particle translate with speed $(\ell^2/\eta)\rho^{f\circ}\boldsymbol{E}$ in a fluid that is otherwise at rest. The particle displacement relative to the skeleton in the far field, however, equals the steady displacement calculated by Mohammadi & Hill (2010) for a skeleton that is at rest in the far field with a steady undisturbed electro-osmotic flow velocity $-(\ell^2/\eta)\rho^{f\circ}\boldsymbol{E}$. Note that the electrophoretic mobility

$$\mu_E = -\mathrm{i}\omega\frac{Z}{E} = \frac{-\mathrm{i}\omega f^E - f^Z(\ell^2/\eta)\rho^{f\circ}}{(\rho - \rho_p)V_p\omega^2 - f^Z} \tag{A 10}$$

is the dynamic electrophoretic mobility defined by O'Brien (1988) for interpreting the electro-acoustic response.

In the main text, however, we report an electrical susceptibility

$$\frac{Z}{E} = \frac{f^E}{(\rho - \rho_p)V_p\omega^2 - f^Z}, \tag{A 11}$$

which satisfies the boundary conditions

$$\boldsymbol{v}' = \boldsymbol{Z} \quad \text{and} \quad \boldsymbol{u}' = -\mathrm{i}\omega\boldsymbol{Z} \quad \text{at} \quad r = a, \tag{A 12}$$

$$\boldsymbol{v}' \to 0 \quad \text{and} \quad \boldsymbol{u}' \to -(\ell^2/\eta)\rho^{f\circ}\boldsymbol{E} \quad \text{as} \quad r \to \infty \tag{A 13}$$

and

$$\nabla p' \to -\mathrm{i}\omega\rho(\ell^2/\eta)\rho^{f\circ}\boldsymbol{E} \quad \text{as} \quad r \to \infty. \tag{A 14}$$

The mobility $-\mathrm{i}\omega Z/E$ is not the foregoing electrophoretic mobility μ_E, because there is a non-zero far-field pressure gradient. Nevertheless, Z/E is the steady particle displacement in an undisturbed skeleton that is stationary at zero frequency, and the particle displacement at finite frequencies is easily interpreted as the displacement relative to a stationary skeleton.

https://doi.org/10.1017/S0022112010005045 Published online by Cambridge University Press

Appendix B. Boundary conditions and equation of motion for dynamic susceptibility

The boundary conditions for the Z-problem are

$$\boldsymbol{v}' = \boldsymbol{u}' = 0 \quad \text{at} \quad r = a, \tag{B 1}$$

$$\boldsymbol{v}' \to -\boldsymbol{Z} \quad \text{and} \quad \boldsymbol{u}' \to \mathrm{i}\omega\boldsymbol{Z} \quad \text{as} \quad r \to \infty \tag{B 2}$$

and

$$\nabla p' \to -\rho\omega^2\boldsymbol{Z} \quad \text{as} \quad r \to \infty. \tag{B 3}$$

Recall that these produce a force $f^Z\boldsymbol{Z}$ on the stationary particle.

To satisfy the boundary conditions for moving particle, we must superpose a rigid-body translation of the particle and hydrogel. The hydrogel equation of motion is simply $-\omega^2\rho\boldsymbol{Z} = -\nabla p^t$, which produces a force $-\nabla p^t V_p$, where $V_p = (4/3)\pi a^3$ is the particle volume. Therefore, superposing all the forces (from the rigid-body translation and the disturbances in the Z-problem) yields an equation of motion

$$-\rho_p V_p\omega^2\boldsymbol{Z} = -\nabla p^t V_p + f^Z\boldsymbol{Z} + \boldsymbol{F}, \tag{B 4}$$

where $\boldsymbol{F}$ is an optical or magnetic force acting on the particle.

We must chose $\nabla p^t = \rho\omega^2\boldsymbol{Z}$ to ensure that the far-field pressure gradient and, hence, the fluid velocity for the combined problem vanishes. It follows that the particle equation of motion is

$$-\rho_p V_p\omega^2\boldsymbol{Z} = -\rho V_p\omega^2\boldsymbol{Z} + f^Z\boldsymbol{Z} + \boldsymbol{F}, \tag{B 5}$$

which yields the ratio Z/F calculated in the main text.

Note that the boundary conditions in the laboratory reference frame are now

$$\boldsymbol{v}' = \boldsymbol{Z} \quad \text{and} \quad \boldsymbol{u}' = -\mathrm{i}\omega\boldsymbol{Z} \quad \text{at} \quad r = a, \tag{B 6}$$

$$\boldsymbol{v}' = \boldsymbol{u}' \to 0 \quad \text{as} \quad r \to \infty \tag{B 7}$$

and

$$\nabla(p' + p^t) \to 0 \quad \text{as} \quad r \to \infty. \tag{B 8}$$

REFERENCES

Ahualli, S., Delgado, A. V., Miklavcic, S. J. & White, L. R. 2007 Use of a cell model for the evaluation of the dynamic mobility of spherical silica suspensions. *J. Colloid Interface Sci.* **309**, 342–349.

Cowin, S. C. & Doty, S. B. 2007 *Tissue Mechanics*. Springer.

Desai, F. N., Hammad, H. R. & Hayes, K. F. 1993 Background electrolyte correction for electrokinetic sonic amplitude measurements. *Langmuir* **9**, 2888–2894.

Dukhin, A. S. & Goetz, P. J. 2001 New developments in acoustic and electroacoustic spectroscopy for characterizing concentrated dispersions. *Colloids Surf.* A*: Physicochem. Engng Asp.* **192** (1–3), 267–306.

Dukhin, A. S., Goetz, P. J., Wines, T. H. & Somasundaran, P. 2000 Acoustic and electroacoustic spectroscopy. *Colloids Surf.* A*: Physicochem. Engng Asp.* **173** (1–3), 127–158.

English, A. E., Tanaka, T. & Edelman, E. R. 1997 Equilibrium and non-equilibrium phase transitions in copolymer polyelectrolyte hydrogels. *J. Chem. Phys.* **107** (5), 1645–1654.

Epstein, P. S. & Carhart, R. R. 1953 The absorption of sound in suspensions and emulsions. Part I. Water fog in air. *J. Acoust. Soc. Am.* **25** (3), 553–565.

Fu, H. C., Shenoy, V. B. & Powers, T. R. 2008 Role of slip between a probe particle and a gel in microrheology. *Phys. Rev.* E **78** (6), 061503.

https://doi.org/10.1017/S0022112010005045 Published online by Cambridge University Press

Gardel, M. L., Valentine, M. T. & Weitz, D. A. 2005 Microrheology. In *Microscale Diagnostics Techniques* (ed. K. Breuer), chapter 1, pp. 1–50. Springer.

de Gennes, P. G. 1976 Dynamics of entangled polymer solutions. Part I. The Rouse model. *Marcromolecules* **9**, 587.

Gu, W. Y., Lai, W. M. & Mow, V. C. 1998 A mixture theory for charged-hydrated soft tissues containing multi-electrolytes: passive transport and swelling behaviors. *J. Biomech. Engng* **120**, 169–180.

Hill, R. J. & Ostoja-Starzewski, M. 2008 Electric-field-induced displacement of a charged spherical colloid embedded in an elastic Brinkman medium. *Phys. Rev.* E **77**, 011404.

Hunter, R. J. 1998 Recent developments in the electroacoustic characterisation of colloidal suspensions and emulsions. *Colloids Surf.* A*: Physicochem. Engng Asp.* **141** (1), 37–65.

Johnson, D. L. 1982 Elastodynamics of gels. *J. Chem. Phys.* **77** (3), 1531–1539.

Klein, M., Andersson, M., Axner, O. & Fällman, E. 2007 Dual-trap technique for reduction of low-frequency noise in force measuring optical tweezers. *Appl. Opt.* **46** (3), 405.

Kollmannsberger, P. & Fabry, B. 2007 High-force magnetic tweezers with force feedback for biological applications. *Rev. Sci. Instrum.* **78**, 114–301.

Lai, W. M., Hou, J. S. & Mow, V. C. 1991 A triphasic theory for the swelling and deformation behaviors of articular cartilage. *J. Biomech. Engng* **113** (3), 245–258.

Landau, L. D. & Lifshitz, E. M. 1987 *Fluid Mechanics*, 2nd edn. Pergamon.

Levine, A. J. & Lubensky, T. C. 2000 One- and two-particle microrheology. *Phys. Rev. Lett.* **85** (8), 1774–1777.

Levine, A. J. & Lubensky, T. C. 2001 Response function of a sphere in a viscoelastic two-fluid medium. *Phys. Rev.* E **63** (4), 041510.

Li, H., Chen, J. & Lam, K. 2006 A transient simulation to predict the kinetic behavior of hydrogels responsive to electric stimulus. *Biomacromolecules* **7** (6), 1951–1959.

Li, H., Chen, J. & Lam, K. Y. 2004*a* Multiphysical modeling and meshless simulation of electric-sensitive hydrogels. *J. Polym. Sci. Part* B*: Polym. Phys.* **42** (8), 1514–1531.

Li, H., Yuan, Z., Lam, K. Y. Lee, H. P., Chen, J., Hanes, J. & Fu, J. 2004*b* Model development and numerical simulation of electric-stimulus-responsive hydrogels subject to an externally applied electric field. *Biosens. Bioelectron.* **19** (9), 1097–1107.

MacKintosh, F. C. & Levine, A. J. 2008 Nonequilibrium mechanics and dynamics of motor-activated gels. *Phys. Rev. Lett.* **100** (1), 018104.

MacKintosh, F. C. & Schmidt, C. F. 1999 Microrheology. *Curr. Opin. Colloid Interface Sci.* **4**, 300–307.

Mason, T. G. & Weitz, D. A. 1995 Optical measurements of frequency-dependent linear viscoelastic moduli of complex fluids. *Phys. Rev. Lett.* **74** (7), 1250–1253.

Mizuno, D., Kimura, Y. & Hayakawa, R. 2001 Electrophoretic microrheology in a dilute lamellar phase of a nonionic surfactant. *Phys. Rev. Lett.* **87** (8), 088104.

Mizuno, D., Kimura, Y. & Hayakawa, R. 2004 Electrophoretic microrheology of a dilute lamellar phase: relaxation mechanisms in frequency dependent mobility of nanometer-sized particles between soft membranes. *Phys. Rev.* E **70**, 011509.

Mohammadi, A. & Hill, R. J. 2010 Steady electrical and micro-rheological response functions for uncharged colloidal inclusions in polyelectrolyte hydrogels. *Proc. R. Soc.* A **466** (2113), 213–235.

Nägele, G. 2003 Viscoelasticity and diffusional properties of colloidal model dispersions. *J. Phys. Condens. Matter* **15** (1), S407–S414.

Nugent-Glandorf, L. & Perkins, T. T. 2004 Measuring 0.1-nm motion in 1 ms in an optical microscope with differential back-focal-plane detection. *Opt. Lett.* **29** (22), 2611.

O'Brien, R. W. 1982 The response of a colloidal suspension to an alternating electric field. *Adv. Colloid Interface Sci.* **16** (1), 281–320.

O'Brien, R. W. 1988 Electro-acoustic effects in a dilute suspension of spherical particles. *J. Fluid Mech.* **190**, 71–86.

O'Brien, R. W. 1990 Electroacoustic equations for a colloidal suspension. *J. Fluid Mech.* **212**, 81–93.

O'Brien, R. W. & White, L. R. 1978 Electrophoretic mobility of a spherical colloidal particle. *J. Chem. Soc. Faraday Trans. II* **74**, 1607–1626.

Pride, S. 1994 Governing equations for the coupled electromagnetics and acoustics of porous media. *Phys. Rev.* B **50** (21), 15678–15696.

https://doi.org/10.1017/S0022112010005045 Published online by Cambridge University Press

Russel, W. B., Schowalter, W. R. & Saville, D. A. 1989 *Colloidal Dispersions*. Cambridge University Press.

Schnurr, B., Gittes, F., MacKintosh, F. C. & Schmidt, C. F. 1997 Determining microscopic viscoelasticity in flexible and semiflexible polymer networks from thermal fluctuations. *Macromolecules* **30**, 7781–7792.

Squires, T. M. & Mason, T. G. 2010 Fluid mechanics of microrheology. *Annu. Rev. Fluid Mech.* **42**, 413–438.

Tanaka, T., Hocker, L. O. & Benedek, G. B. 1973 Spectrum of light scattered from a viscoelastic gel. *J. Chem. Phys.* **59** (9), 5160–5183.

Tanaka, T., Ishiwata, S. & Ishimoto, C. 1977 Critical behavior of density fluctuations in gels. *Phys. Rev. Lett.* **38** (14), 771–774.

Temkin, S. 2005 *Suspension Acoustics: An Introduction to the Physics of Suspensions*, 1st edn. Cambridge University Press.

Waigh, T. A. 2005 Microrheology of complex fluids. *Rep. Prog. Phys.* **68**, 685–742.

Wang, M. & Hill, R. J. 2008 Electric-field-induced displacement of a charged spherical colloid embedded in a Brinkman medium. *Soft Matter* **4**, 1048–1058.

Wang, M. & Hill, R. J. 2009 Dynamic electric-field-induced response of charged spherical colloids in uncharged hydrogels. *J. Fluid Mech.* **640**, 357–400.

Xu, K., Forest, M. G. & Klapper, I. 2007 On the correspondence between creeping flows of viscous and viscoelastic fluids. *J. Non-Newton. Fluid Mech.* **145** (2–3), 150–172.

Yariv, E. 2006 'Force-free' electrophoresis? *Phys. Fluids* **18** (3), 031702.

Zwanzig, R. & Bixon, M. 1970 Hydrodynamic theory of the velocity correlation function. *Phys. Rev.* A **2** (5), 2005–2012.

https://doi.org/10.1017/S0022112010005045 Published online by Cambridge University Press